

Igneous breccia in the West Timbered Hills, Arbuckle Mountains: Origin from explosive basaltic phreatomagmatic processes

Amy M. Eschberger¹ and Richard E. Hanson²

¹*School of Geology, Energy, and the Environment, Texas Christian University, Fort Worth, Texas 76129. Current address: Colorado Department of Natural Resources, Division of Reclamation, Mining, and Safety, 1313 Sherman Street, Suite 215, Denver, Colorado 80203. aeschberger@yahoo.com.*

²*School of Geology, Energy, and the Environment, Texas Christian University, Fort Worth, Texas 76129. r.hanson@tcu.edu. Corresponding author.*

INTRODUCTION

In the West Timbered Hills in the Arbuckle Mountains, a quarry run by Hanson Aggregates, Inc., exposes an unusual, coarse-grained polymict igneous breccia that contains a variety of mafic and felsic igneous clasts and occurs within the Carlton Rhyolite Group <1 km southwest of the Washita Valley Fault Zone (fig. 2 in Eschberger et al., this guidebook). No other examples of this type of breccia have been documented from other parts of the Wichita Igneous Province. The breccia is associated with a series of diabase intrusions. It is not shown on any published geologic map of the region but probably has a width of ≥ 1 km, based on the current dimensions of the quarry. The Upper Cambrian Reagan Sandstone unconformably overlies the breccia.

Uhl (1932) provided an early description of the breccia in the area now occupied by the quarry. He noted that the breccia contains abundant clasts of felsic volcanic rock intermixed with diabase and proposed that the breccia formed when a mafic lava flow incorporated the felsic clasts as it moved across the surface. A more complete description of the breccia was included as a field-trip stop in the guidebook by Price et al. (1998), who demonstrated that the Carlton Rhyolite and some of the diabase intrusions are faulted against the breccia. They also showed that the breccia locally appears to be concordant with layering in underlying Carlton Rhyolite in one area along the west quarry wall. Based on their observations, they suggested that the breccia either represents the fill of a volcanic vent or a xenolith-rich flow in a near-vent setting and inferred that interactions between external water and intrusive mafic magma at some depth beneath the surface caused an explosive eruption.

Elmore et al. (1998) and Price et al. (1998) documented fairly extensive hydrothermal alteration of the breccia, the adjacent Carlton Rhyolite, and the intrusive diabase,

which included formation of significant amounts of secondary carbonate. Price et al. (1998) ascribed the alteration to ingress of fluids that had interacted with the extensive Cambro-Ordovician carbonate strata deposited on top of the rhyolites and inferred that fluid migration might have occurred during basin subsidence after the cessation of igneous activity or when the Wichita igneous rocks were thrust over the carbonate strata in the late Paleozoic. Paleomagnetic data indicate that a significant part of the alteration occurred during late Paleozoic deformation (Elmore et al., 1998). In any case, proximity to the Washita Valley Fault system presumably facilitated the fluid migration.

Our study of the breccia is based on a suite of samples collected from loose blocks on the quarry floor during a single visit to the quarry. Because of safety considerations we were unable to approach the quarry walls and cannot add meaningfully to the field observations made by Price et al. (1998). However, we have carried out a petrographic study of 41 thin sections from the breccia matrix and clasts within the breccia, which allows us to build on some of the conclusions reached by Price et al. (1998). We also present major- and trace-element analyses for four new samples from the quarry (Table 1). For additional details on our sample suite, the reader is referred to Eschberger (2012).

DIABASE INTRUSIONS

A number of diabase intrusions cut the igneous breccia in the quarry walls. The smaller intrusions are dikes as thick as a few meters that have variable orientations. The largest intrusion is a massive diabase body visible on the west wall of the quarry. It is estimated to be ~ 200 m across and has a high-angle contact against the adjacent breccia. In thin section, a sample from the intrusion contains plagioclase laths ≤ 2.5 mm in length that are partly replaced by very fine grained pumpellyite, green clay, and carbonate.

TABLE 1: GEOCHEMICAL DATA FOR WEST TIMBERED HILLS QUARRY SAMPLES

| | Microgranite Clast | Rhyolite Clast | Diabase Clast | Diabase Intrusion |
|--|-----------------------|-------------------|------------------|----------------------|
| Normalized major elements (wt %)* | | | | |
| Sample: | HQ-1 | HQ-4 | HQ-2 | HQ-3 |
| SiO ₂ | 69.63 | 70.03 | 51.26 | 54.17 |
| TiO ₂ | 0.90 | 1.02 | 4.18 | 3.31 |
| Al ₂ O ₃ | 12.41 | 12.46 | 14.20 | 13.16 |
| FeO | 5.12 | 4.97 | 14.17 | 12.66 |
| MnO | 0.09 | 0.07 | 0.37 | 0.21 |
| MgO | 0.92 | 1.26 | 4.54 | 3.57 |
| CaO | 2.39 | 2.48 | 5.64 | 6.74 |
| Na ₂ O | 3.57 | 3.69 | 3.80 | 3.89 |
| K ₂ O | 4.75 | 3.79 | 1.30 | 1.66 |
| P ₂ O ₅ | 0.21 | 0.23 | 0.54 | 0.64 |
| LOI** | 1.23 | 1.61 | 4.73 | 1.74 |
| Total*** | 98.29 | 97.09 | 94.31 | 97.83 |
| Trace elements (ppm) | | | | |
| Ni | 2.29 | 2.79 | 28.91 | 0.90 |
| Cr | 0.00 | 2.09 | 2.39 | 0.00 |
| Sc | 9.76 | 10.57 | 36.39 | 26.52 |
| V | 29.91 | 51.15 | 395.11 | 242.57 |
| Ba | 798.03 | 944.78 | 348.54 | 512.95 |
| Rb | 110.06 | 88.03 | 30.15 | 32.00 |
| Sr | 170.44 | 222.12 | 219.02 | 377.66 |
| Zr | 541.49 | 515.57 | 334.61 | 320.19 |
| Y | 65.41 | 63.19 | 48.52 | 48.30 |
| Nb | 41.42 | 39.85 | 28.17 | 27.70 |
| Ga | 14.46 | 14.86 | 28.91 | 22.93 |
| Cu | 21.54 | 33.20 | 140.58 | 16.65 |
| Zn | 98.60 | 89.23 | 156.73 | 149.85 |
| Pb | 11.02 | 4.60 | 3.10 | 6.55 |
| La | 63.19 | 60.74 | 34.63 | 36.70 |
| Ce | 141.18 | 136.51 | 80.02 | 83.83 |
| Th | 8.20 | 8.07 | 3.47 | 3.26 |
| Nd | 67.68 | 65.64 | 47.77 | 50.03 |
| U | 2.03 | 1.98 | 0.90 | 0.83 |
| Pr | 17.21 | 16.70 | 11.03 | 11.52 |
| Sm | 14.72 | 14.16 | 11.77 | 12.10 |
| Eu | 2.89 | 2.70 | 2.47 | 3.51 |
| Gd | 13.34 | 12.85 | 11.26 | 11.51 |
| Tb | 2.21 | 2.11 | 1.81 | 1.81 |
| Dy | 13.06 | 12.39 | 10.47 | 10.22 |
| Ho | 2.62 | 2.49 | 2.03 | 1.98 |
| Er | 6.88 | 6.65 | 5.08 | 4.94 |
| Tm | 1.01 | 0.96 | 0.71 | 0.67 |
| Yb | 6.11 | 5.95 | 4.16 | 3.96 |
| Lu | 0.91 | 0.90 | 0.61 | 0.60 |
| Hf | 13.71 | 13.14 | 8.70 | 8.23 |
| Ta | 2.62 | 2.55 | 1.83 | 1.78 |
| Cs | 0.32 | 0.31 | 0.14 | 0.15 |

* Major elements are normalized to 100% on a volatile-free basis

** Loss on ignition ***Total before normalization

Augite is relatively fresh, and a few mafic crystals completely replaced by green clay are inferred to represent original olivine, based on crystal shapes (Figs. 1A and 1B). Magnetite is the dominant Fe-Ti oxide and occurs with blades of ilmenite. The diabase is relatively leucocratic and contains microveinlets of very fine grained, intergrown quartz, K-feldspar, and plagioclase (Fig. 1C), representing low-temperature differentiated magma produced during final stages of crystallization. A chemical analysis of the diabase is given in Table 1 (sample HQ-3).

GENERAL CHARACTERISTICS OF THE BRECCIA

The breccia is very poorly sorted and clast- to matrix-supported, with fragments ranging from >1 m across down to irresolvable dust between the coarser particles (Figs. 2 and 3). Different textural types of microgranite, rhyolite, diabase, and basalt make up the coarser clasts. Price et al. (1998) also reported clasts of monzonite/syenite, but we did not encounter these rock types in our study, suggesting that clast compositions vary in different parts of the breccia. The coarser clasts typically range from angular to subrounded. Large pieces of the breccia on the quarry floor are massive and show no stratification. However, crude, meter-scale, moderately dipping layering is visible in places in the breccia on the quarry walls.

The breccia matrix consists of a chaotic mixture of fragments that vary in composition, size, and alteration (Figs. 2B, 2C and 3). In thin section, crystal and lithic fragments <1 mm in size occupy much of the matrix and are angular to subangular. Some areas of the matrix show a high abundance of felsic material in the form of rhyolite lithic debris and quartz and alkali-feldspar crystals and crystal fragments. Mafic material, however, is generally dominant and consists of diabase and basalt clasts and crystals and crystal fragments of plagioclase and augite.

Clast types in the breccia

Rhyolite

Chemical and modal analyses of representative rhyolite and microgranite clasts are given in Tables 1 and 2. The color of the rhyolite clasts ranges from dark brown-red to pale pink depending on the amount of hematite dusting present. All of the rhyolite in the breccia is porphyritic and shows variable amounts and sizes of phenocrysts and glomerocrysts. Plagioclase phenocrysts (variably altered to carbonate and epidote) are the most common (Figs. 4A and 4B),

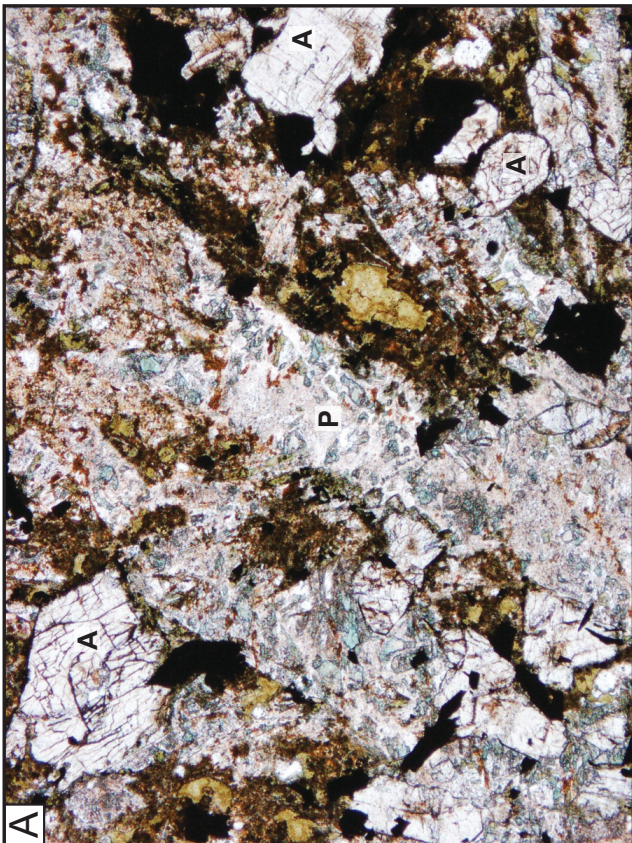
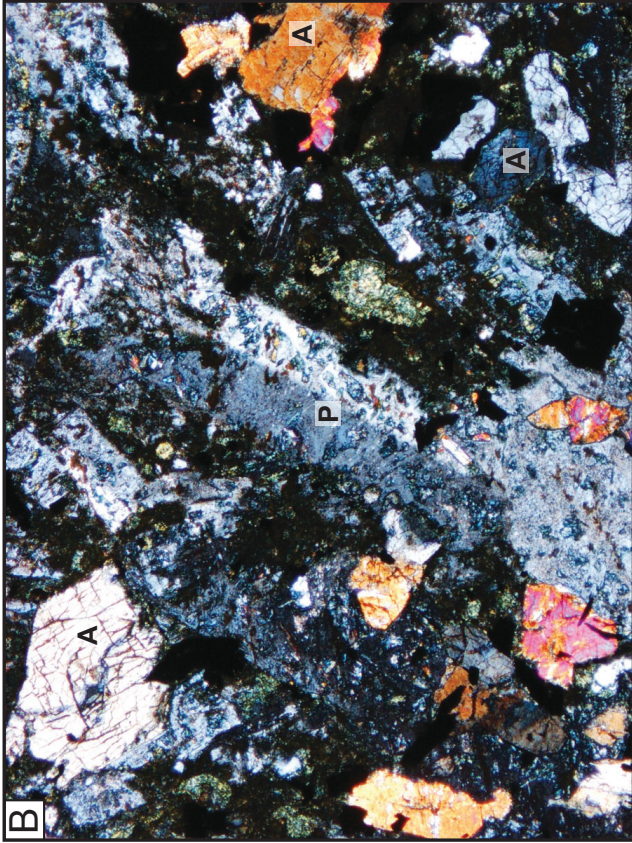


Figure 1. (A) Photomicrograph of diabase sample HQ-3 showing relatively fresh augite (A) and plagioclase (P) partly altered to relatively blue-green pumpellyite and brownish-green clay. Plane-polarized light; field of view ~2.5 mm across. (B) Same view as Figure 1A under crossed polars. Pumpellyite shows anomalous blue and brown interference colors. Field of view ~2.5 mm across. (C) Photomicrograph of diabase sample HQ-3 showing quartzofeldspathic veinlet (V) in lower left. Plane-polarized light; field of view ~5 mm across.

TABLE 2: MODAL ANALYSES OF FELSIC CLASTS IN IGNEOUS BRECCIA

| Sample | Points counted in thin section | Feldspar (%) | Mafic silicate pseudomorphs (%) | Titanomagnetite (%) | Groundmass (%) | Maximum feldspar size (mm) | Maximum mafic silicate pseudomorph size (mm) | Maximum titanomagnetite size (mm) | Maximum glomerocryst size (mm) |
|--------|--------------------------------|--------------|---------------------------------|---------------------|----------------|----------------------------|--|-----------------------------------|--------------------------------|
| HQ-1 | 1530 | 32.7 | 5.5 | 4.6 | 57.2 | 3 | 1 | 0.25 | 6 |
| HQ-4 | 1620 | 4.6 | 2.5 | 2.9 | 88.8 | 3 | 1.2 | 0.2 | 1.6 |

Point counts were done on standard thin sections; mafic silicate pseudomorphs include partly unaltered augite in sample HQ-1. Sample HQ-1 is a microgranite; sample HQ-4 is a rhyolite.

and larger, partially resorbed alkali-feldspar phenocrysts and variably altered mafic silicate phenocrysts occur in lesser amounts. Well-preserved augite phenocrysts are present in some samples (Fig. 4A), but the mafic silicates have generally been completely replaced by green clay, carbonate, and epidote. The shapes of the pseudomorphs suggest that they were mostly originally pyroxene, but amphibole phenocrysts were also originally present based on relict cleavage traces in some pseudomorphs. Titanomagnetite occurs as tiny grains dispersed throughout the groundmass or as coarser glomerocrysts consisting of several grains. More complex glomerocrysts are also present and consist mostly of feldspar together with some titanomagnetite, mafic silicate pseudomorphs, and accessory apatite.

Many of the rhyolite clasts are spherulitic. Individual spherulites range from <0.25 mm to ~1.25 mm in diameter (Figs. 4B and 4C) and are typically rimmed by hematite dust (Fig. 4C). Minor amounts of roughly spherical amygdules as large as ~2.5 mm across also occur and are filled with quartz or less commonly with carbonate. Other rhyolite clasts show felsitic texture with randomly oriented tridymite needles (now inverted to quartz) of the same type that is so commonly present in the Carlton Rhyolite in other areas (Fig. 4D). The tridymite needles range in length from <0.25 mm to 1 mm in different clasts. Some clasts contain long, slender aegirine or aegirine-augite crystals with characteristic green pleochroism (Fig. 5A), indicating a peralkaline composition for these clasts.

One rhyolite clast ~6.5 cm across within the breccia is actually a breccia itself and contains angular fragments within a partly silicified matrix (Fig. 5B). All of the fragments consist of a single type of dark-red, spherulitic rhyolite, similar to that making up some of the other rhyolite clasts within the breccia. This breccia clast may have been derived from a zone of flow breccia within the Carlton Rhyolite but could also represent an early stage of explosive fragmentation during formation of the main breccia mass.

Microgranite

Microgranite clasts are less common in the breccia than rhyolite clasts. The microgranite clasts in the samples we studied show some variation in grain size but have similar mineralogy and were probably derived from a single intrusion. The main phenocrysts are plagioclase, partly preserved augite, and titanomagnetite. Glomerocrysts consisting generally of ten to 15 individual crystals of these minerals are also present (Fig. 5C) and include small amounts of apatite. These glomerocrysts are as much as ~6 mm across and may have formed by sidewall crystallization in the parent magma chamber. Alteration assemblages are similar to those in the rhyolite clasts.

The phenocrysts and glomerocrysts are set in a very fine grained but phaneritic groundmass. Spherulites as much as 1.4 mm across and tridymite needles to 1 mm in length occur within the groundmass with interstitial anhedral quartz, feldspar, and microgranophyre (Fig. 5D). The textures point to hypabyssal emplacement and are comparable to those seen in many of the felsic hypabyssal intrusions in the East Timbered Hills (Eschberger et al., this guidebook). The microgranite differs from the felsic intrusions in that area, however, in its lack of quartz phenocrysts and the lower abundance of microgranophyre in the groundmass.

Diabase

Diabase clasts are present in all parts of the breccia examined and show a range of textures. Plagioclase and augite are the principal minerals, with lesser amounts of magnetite and bladed ilmenite crystals. Some of the diabase contains amygdules as much as 2 mm across filled with quartz, carbonate, epidote, and green clay. Porphyritic diabase contains plagioclase phenocrysts in a fine-grained intergranular groundmass, and coarser grained diabase shows subophitic to ophitic textures. Sample HQ-2 in Table 1 represents a subophitic diabase clast. Plagioclase and augite show various degrees of alteration to epidote, green clay, and carbonate.

Small amounts of microgranophyre typically occur in interstices between the plagioclase laths, and microveinlets of the same type of differentiated felsic material are present in one diabase clast and are comparable to those seen in the large diabase intrusion (e.g., Fig. 1C). A more

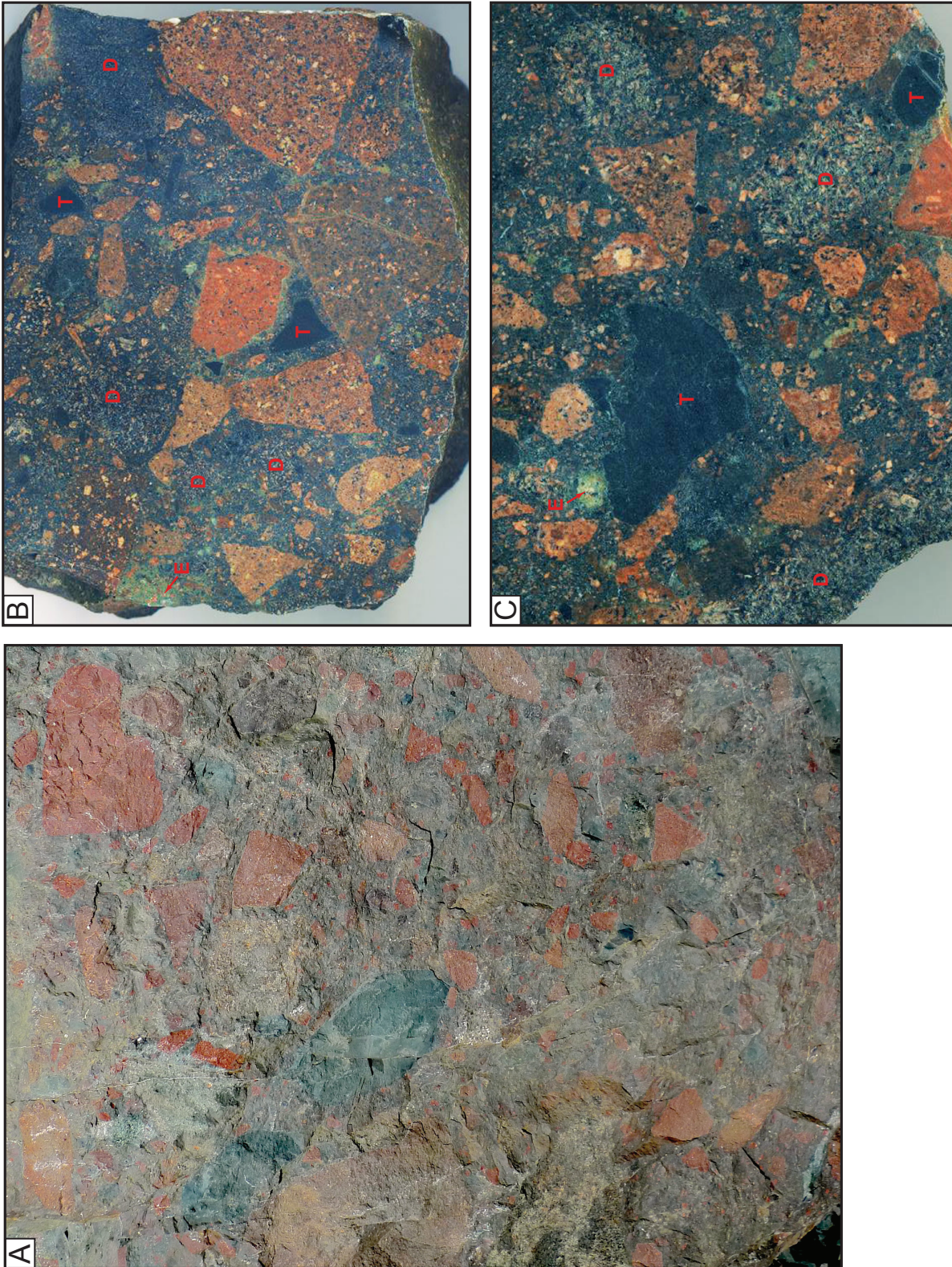


Figure 2. (A) Igneous breccia exposed on loose block on quarry floor (photograph by Bob Puckett). Dark-gray clasts are basalt and diabase; red-brown clasts are rhyolite and microgranite. Secondary epidote is visible in places. Photograph is 44 cm across. (B) Cut slab of breccia showing secondary epidote (E) and clasts of dark-brown to orange porphyritic rhyolite, black tachylite (T), and diabase (D). Photograph is ~20 cm across. (C) Another cut slab of breccia showing similar types of clasts and secondary epidote as in Figure 2B. Photograph is ~15 cm across.

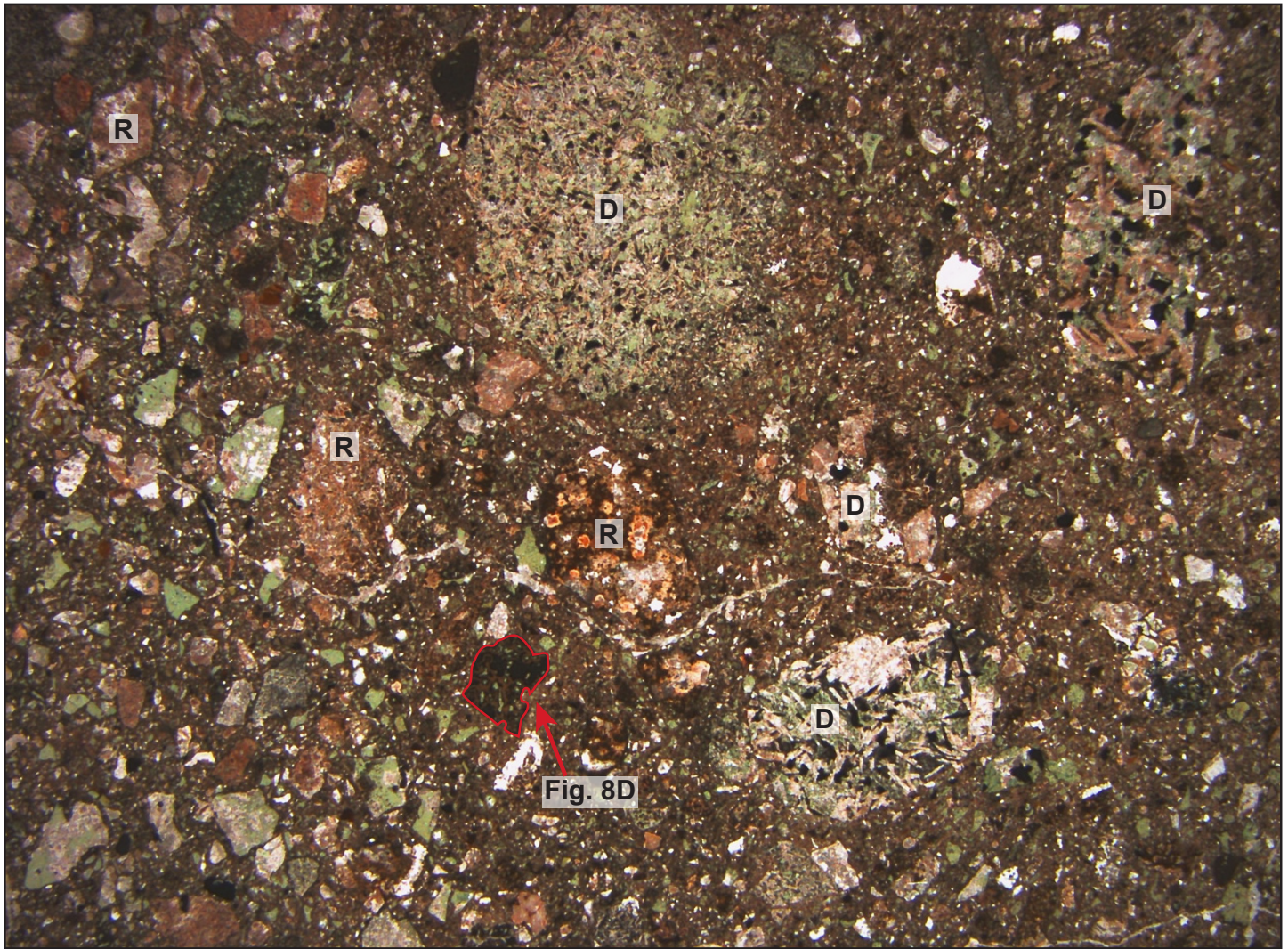


Figure 3. Photomicrograph of breccia matrix showing abundant sideromelane shards altered to green clay and less abundant dark tachylite shards, including example outlined in red and shown in Figure 8D. *R*: rhyolite clasts; *D*: diabase clasts. Plane-polarized light; field of view 2 cm across.

pronounced example of felsic segregations occurs in another diabase clast that has typical subophitic texture but also contains fluidal, irregularly shaped bodies of felsic material that are as much as ~8 cm across and show gradational contacts against the host diabase (Fig. 6A). In thin section, these felsic segregations consist of a very fine grained intergrowth of quartz and K-feldspar showing some microgranophyric texture (Fig. 6B). The centers of the larger felsic segregations are occupied by abundant small, ovoid amygdules filled with quartz (Figs. 6B and 6C). In places, coalescence of vesicles produced larger, more irregularly shaped gas cavities (Fig. 6C). In a few cases, plagioclase

laths in the adjacent diabase are oriented roughly parallel to the margins of the felsic segregations (Fig. 6B). These segregations are somewhat similar to the felsic microveinlets found in the large diabase intrusion, but in the present case the felsic material is more pervasive and is readily visible on the hand-sample scale. The segregations are inferred to have formed from small amounts of low-density, vesiculating felsic magma that rose upward within a solidifying intrusion (e.g., Zavala et al., 2011).

Another large diabase clast shows local areas of plagioclase crystal alignment and bands of magnetite grains (Figs. 6D and 7A), suggesting that this clast came from a

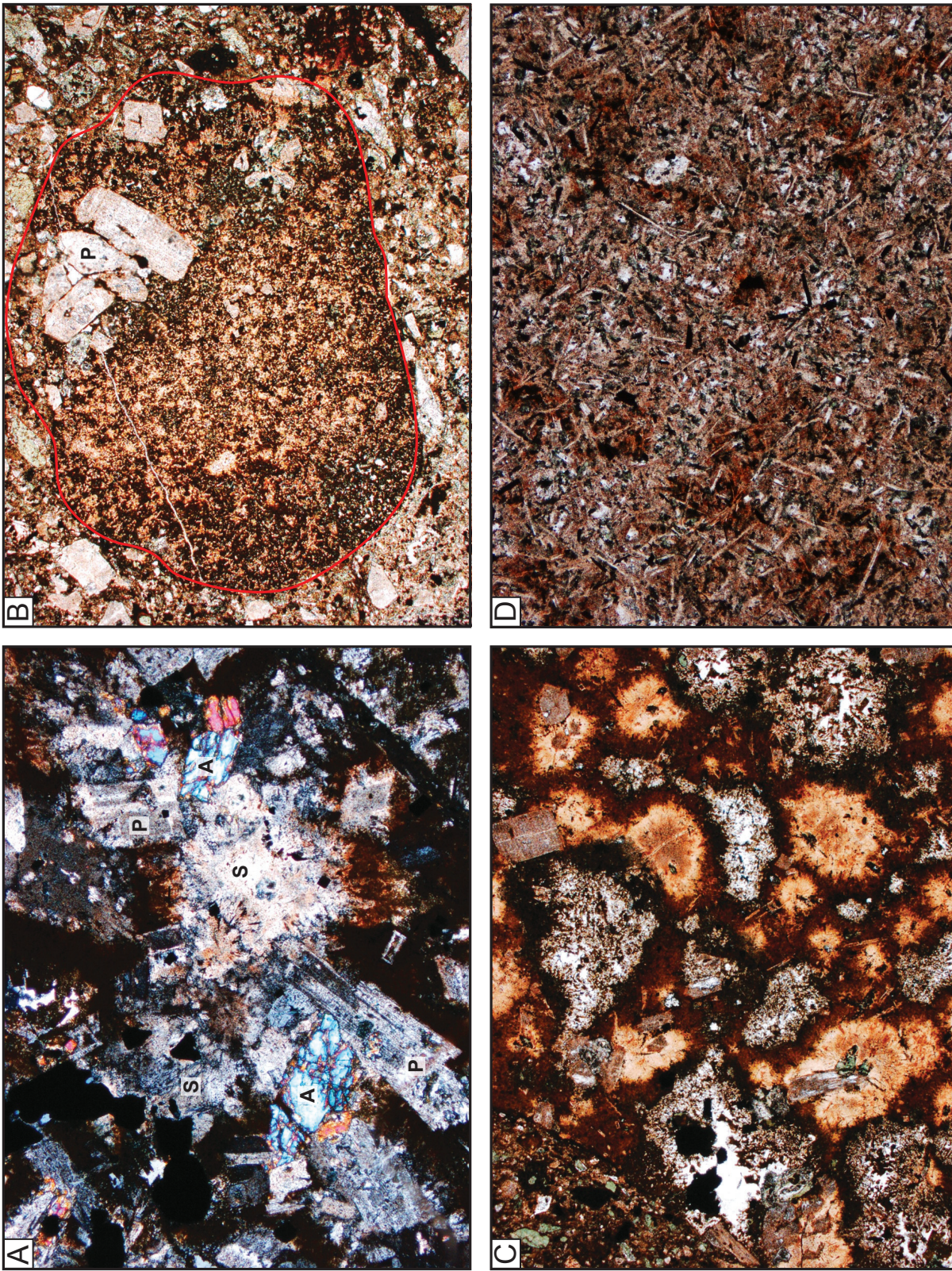


Figure 4. (A) Photomicrograph of rhyolite clast in breccia showing well-preserved, subhedral augite crystals (*A*) intergrown with plagioclase (*P*) in glomerocrysts. *S*: spherulites in groundmass. Crossed polars; field of view ~5 mm across. (B) Photomicrograph of rhyolite clast in breccia (outlined) showing very fine grained spherulitic texture. Plagioclase (*P*) phenocrysts and glomerocryst are also visible. Plane-polarized light; field of view ~5 mm across. (C) Photomicrograph of rhyolite clast in breccia showing relatively coarse grained spherulitic texture. Spherulites are rimmed by hematite dust. Plane-polarized light; field of view ~5 mm across. (D) Photomicrograph of rhyolite clast in breccia showing randomly oriented tridymite needles in felsitic groundmass. Plane-polarized light; field of view ~5 mm across.

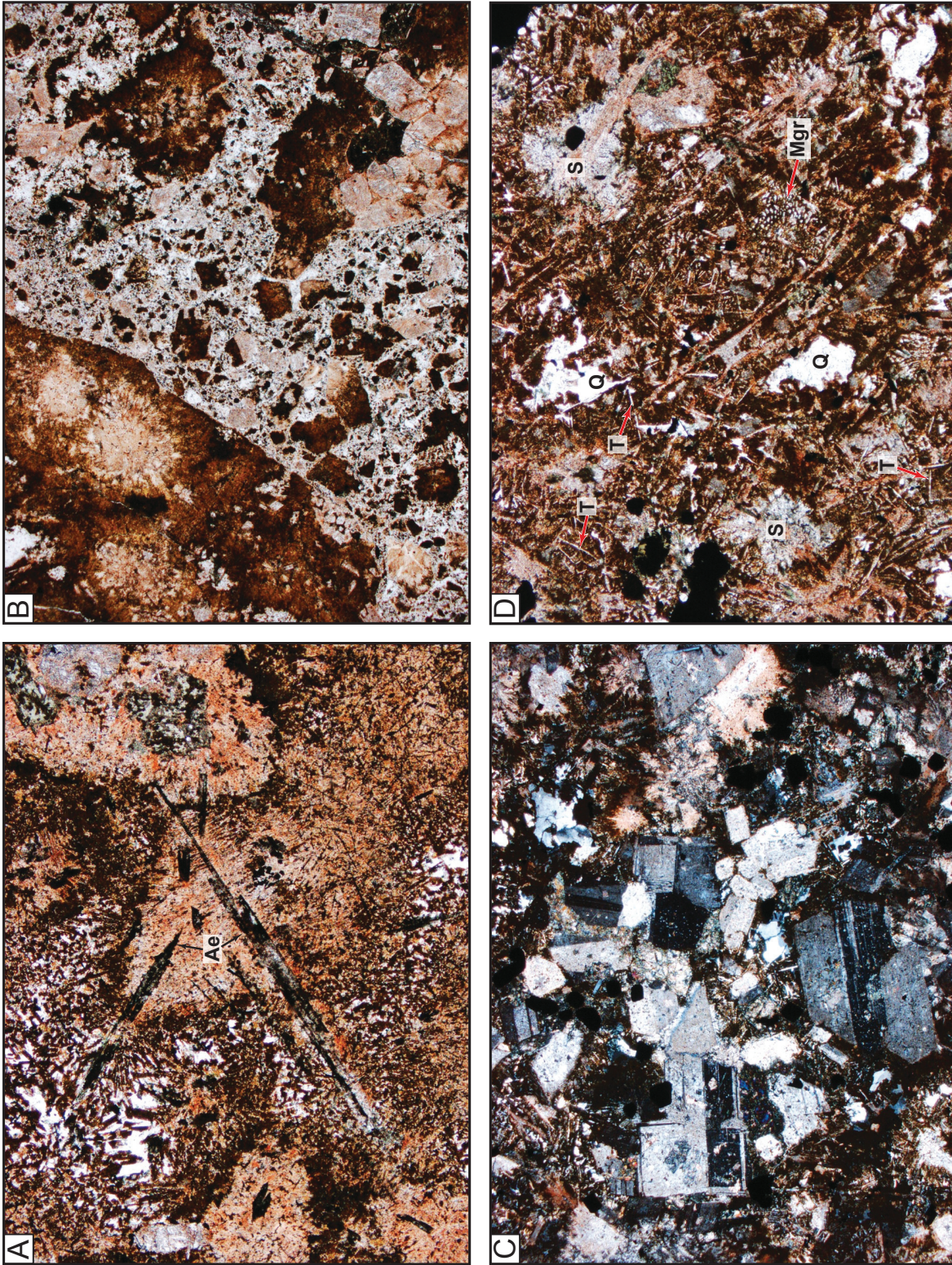


Figure 5. (A) Photomicrograph of rhyolite clast in breccia showing green aegirine or aegirine-augite crystals (*Ae*). Plane-polarized light; field of view ~2.5 mm across. (B) Photomicrograph of rhyolite breccia containing fragments of dark-red spherulitic rhyolite. Plane-polarized light; field of view ~5 mm across. (C) Photomicrograph of microgranite clast (sample HQ-1, Table 1) showing glomerocryst composed of numerous phenocrysts of plagioclase and titanomagnetite. Crossed polars; field of view ~5 mm across. (D) Photomicrograph of microgranite clast (sample HQ-1) showing spherulites (*S*), randomly oriented tridymite needles (*T*), and interstitial anhedronal quartz (*Q*) and microgranophyre (*Mgr*). Plane-polarized light; field of view ~2.5 mm across.

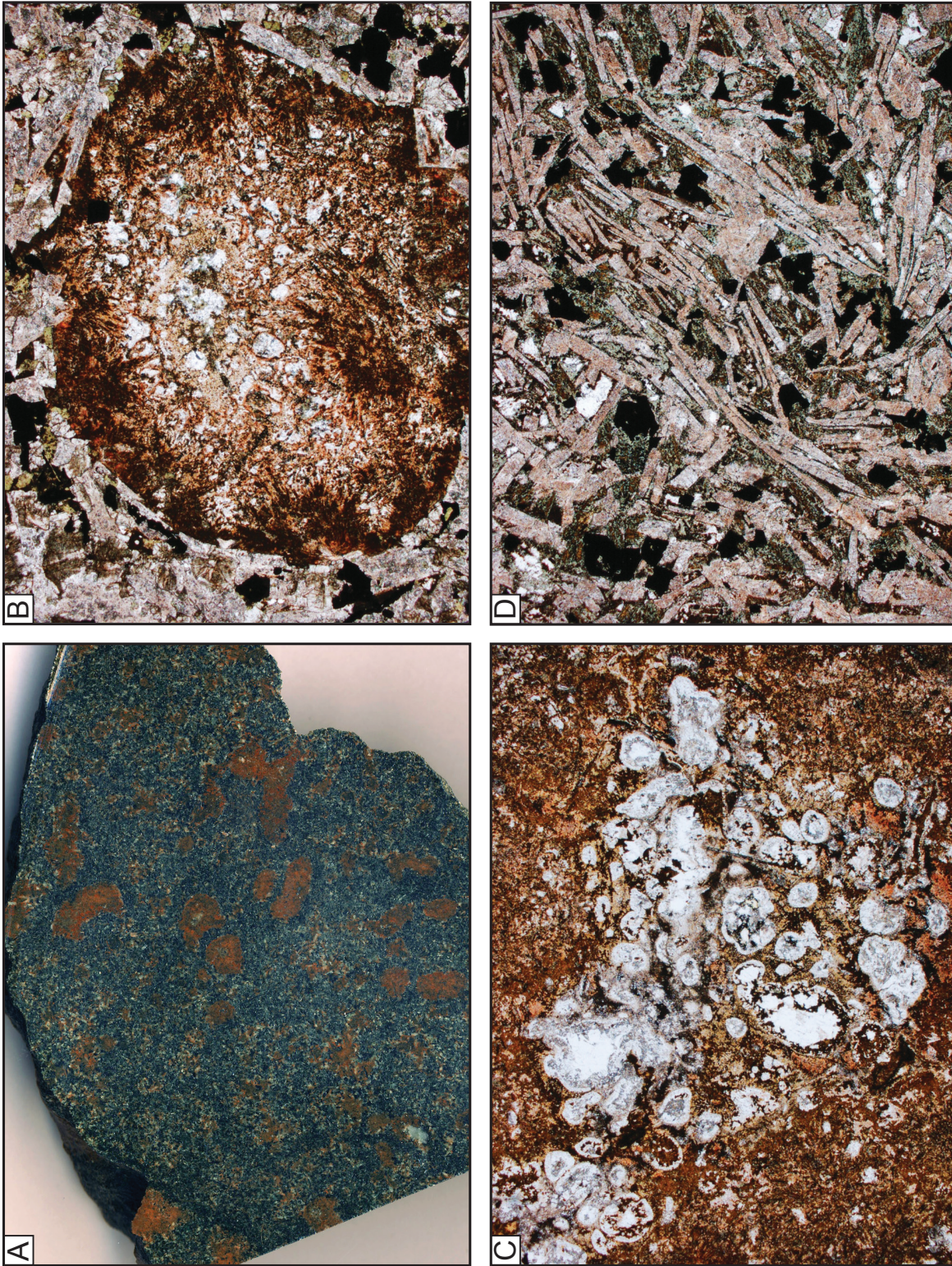


Figure 6. (A) Cut slab of diabase clast showing fluidal, irregularly shaped orange-brown felsic segregations with gradational contacts against host rock. Photograph is ~15 cm across. (B) Photomicrograph showing very fine grained, partly microgranophyric quartz and K-feldspar within felsic segregation. Note ovoid, quartz-filled amygdules in center of segregation and alignment of plagioclase crystals in host diabase parallel to edge of segregation. Plane-polarized light; field of view ~5 mm across. (C) Photomicrograph showing felsic segregation with abundant ovoid, quartz-filled amygdules in its center. Larger, more irregular amygdules represent several smaller vesicles that coalesced during exsolution of gas. Plane-polarized light; field of view ~5 mm across. (D) Photomicrograph of diabase clast showing alignment of plagioclase laths. Plane-polarized light; field of view ~1.3 mm across.

mafic intrusion that developed igneous layering. Overall, these features suggest that the diabase clasts in the breccia were derived from one or more intrusions that were large enough to undergo some internal differentiation.

Basalt

Groundmass textures in basalt lithic clasts in the breccia include variolitic, hyalopilitic, intersertal, and intergranular, recording a wide range in cooling rates [see Puckett et al. (this guidebook) for additional discussion of some of these textural types and their significance]. Some of the basalt clasts may represent juvenile samples of the magma that was involved in the explosive processes leading to breccia formation. At least some of the clasts are not juvenile, however, because they are cut by quartz veinlets that are truncated at clast margins, indicating that the basalt had cooled and experienced secondary mineralization before being fragmented. Plagioclase phenocrysts occur in some clasts (Fig. 7B) and are partially or completely altered to carbonate. Spherical to elongate amygdules are also present and are filled with quartz, carbonate, and green clay. Variolitic texture in some clasts is defined by radiating plagioclase microlites (Fig. 7C) and in other cases by acicular, radiating pyroxene crystals replaced by green clay and magnetite (Fig. 7D); swallow-tailed plagioclase occurs in clasts with pyroxene variolites (Fig. 7D). These types of textures indicate rapid quenching of basalt magma in contact with external water (Bryan, 1972; Shelley, 1993).

An important type of basalt clast that is common in the breccia matrix consists of originally glassy sideromelane or tachylite fragments that are ≤ 5 mm in length and have angular to fluidal shapes (Figs. 3, 8, and 9). The fragments show a range in vesicularity, but their outlines are not controlled by broken bubble walls. Sideromelane clasts, which originally consisted of transparent light-brown basalt glass, are altered in some cases to green clay (Figs. 3 and 8A), but many have been replaced by yellow-brown to brown palagonite (Figs. 8C, 8D, and 9).

Alteration

Palagonite records an early type of alteration in clasts originally consisting of highly unstable sideromelane glass. Evidence for subsequent alteration stages in the breccia includes the presence of veinlets filled with quartz, carbonate, and less abundant chlorite and epidote, which in some cases occur only within particular clasts (representing pre-fragmentation alteration) and in other cases cut across both the matrix and multiple clasts (representing post-fragmentation alteration). Individual clasts in some cases show multiple stages of pre-fragmentation alteration.

For example, one spherulitic rhyolite clast shows a quartz-filled veinlet cross-cutting a chlorite veinlet, both of which terminate at the edge of the clast. The clast and the adjacent matrix are both cut by a carbonate veinlet.

This pattern is consistent with the paragenetic sequence of secondary mineralization documented by Elmore et al. (1998) and Price et al. (1998) in the quarry rocks involving an early stage of quartz and chlorite mineralization followed by two or more stages of carbonate mineralization. In most thin sections of the breccia matrix, carbonate is the youngest and most abundant secondary mineral filling veinlets and centers of amygdules and replacing primary igneous minerals, which in some cases show previous replacement by green clay, chlorite, or epidote. In comparison with the rhyolites and diabases in the East Timbered Hills, the constituents of the igneous breccia show far less sericitic alteration.

GEOCHEMISTRY

Rhyolite and Microgranite

The analyzed rhyolite and microgranite clasts in Table 1 contain minor amounts of quartz- and carbonate-filled amygdules as much as 1.4 mm across, and plagioclase phenocrysts show some replacement by carbonate and epidote. The generally low degree of alteration seen in thin section makes it unlikely that the primary magmatic compositions of these samples have been disturbed to any significant degree. They have similar major-element contents to each other but are lower in silica and higher in CaO, MgO, FeO, TiO₂, and P₂O₅ than any of the rhyolites we have analyzed in the East Timbered Hills (Fig. 10), and they plot in the rhyodacite/dacite field in the Winchester and Floyd (1977) diagram shown in Figure 11A. There is, however, abundant alkali-feldspar in the groundmass of both samples, indicating that they are most appropriately termed rhyolite (or microgranite).

The two samples have very similar contents of immobile trace elements, causing them to cluster tightly in the discrimination diagrams in Figure 11, as well as in the bivariate trace-element plots shown in Figure 12. Note also that their patterns in the multi-element and REE diagrams in Figure 13 are nearly identical. We therefore infer that these rocks represent magmas derived from the same magma chamber, with the microgranite being a hypabyssal intrusive counterpart of the rhyolite. In keeping with their less-evolved major-element compositions, the two clasts show less-fractionated overall trace-element patterns than the felsic rocks in the East Timbered Hills (Fig. 13A). They also generally have lower overall REE contents except for Eu, which is strongly depleted in the more fractionated samples from the East

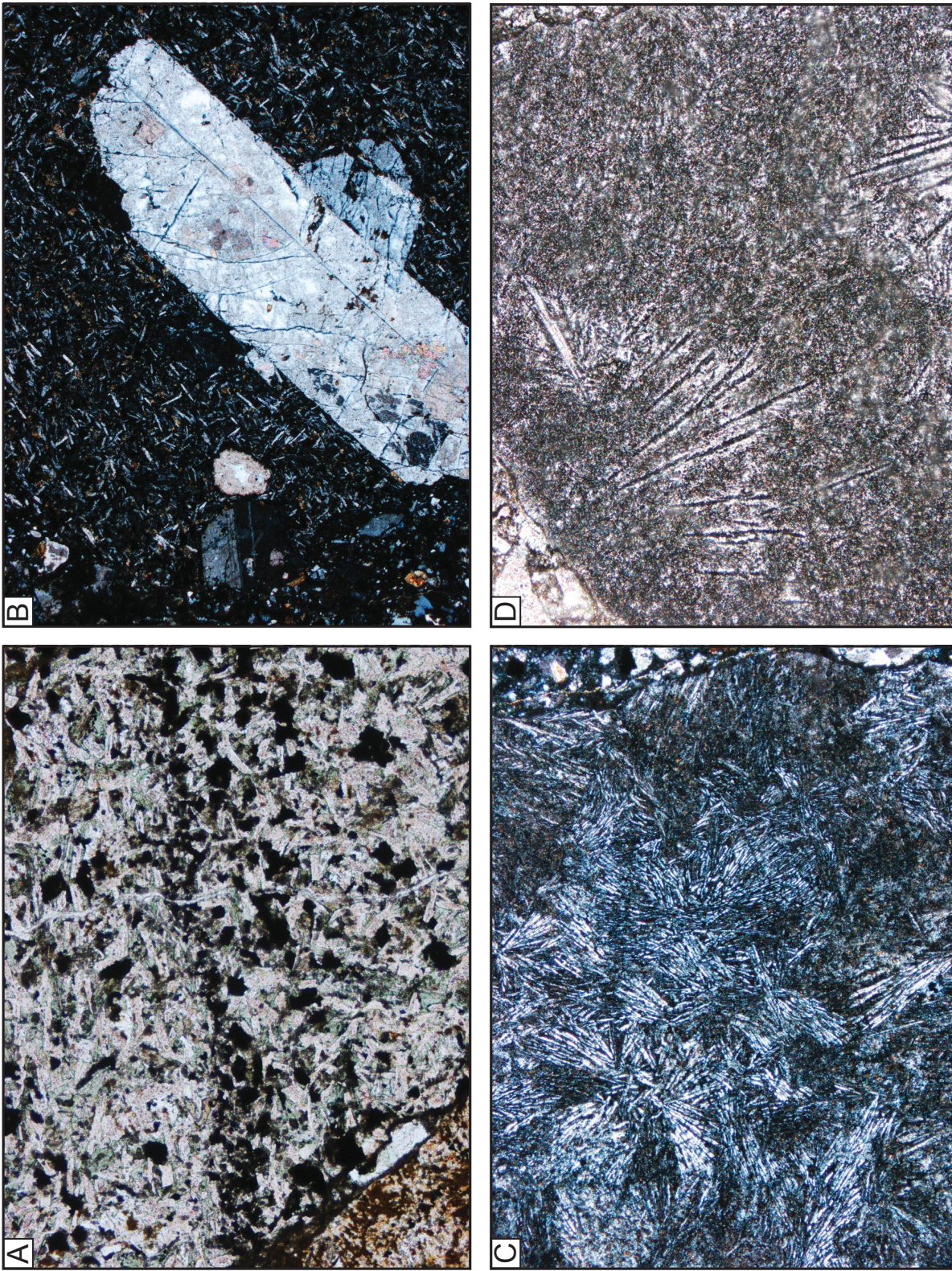


Figure 7. (A) Photomicrograph of diabase clast showing band of magnetite grains and some alignment of plagioclase laths. Plane-polarized light; field of view ~5 mm across. (B) Photomicrograph of porphyritic basalt clast with plagioclase phenocrysts partly altered to calcite. Groundmass shows intergranular texture. Crossed polars; field of view ~5 mm across. (C) Photomicrograph of basalt clast showing variolitic texture defined by radiating plagioclase microclines. Crossed polars; field of view ~5 mm across. (D) Photomicrograph of basalt clast showing variolitic texture with acicular radiating pyroxene crystals. A swallow-tailed plagioclase microcline is visible at top center. Plane-polarized light; field of view ~2.5 mm across.

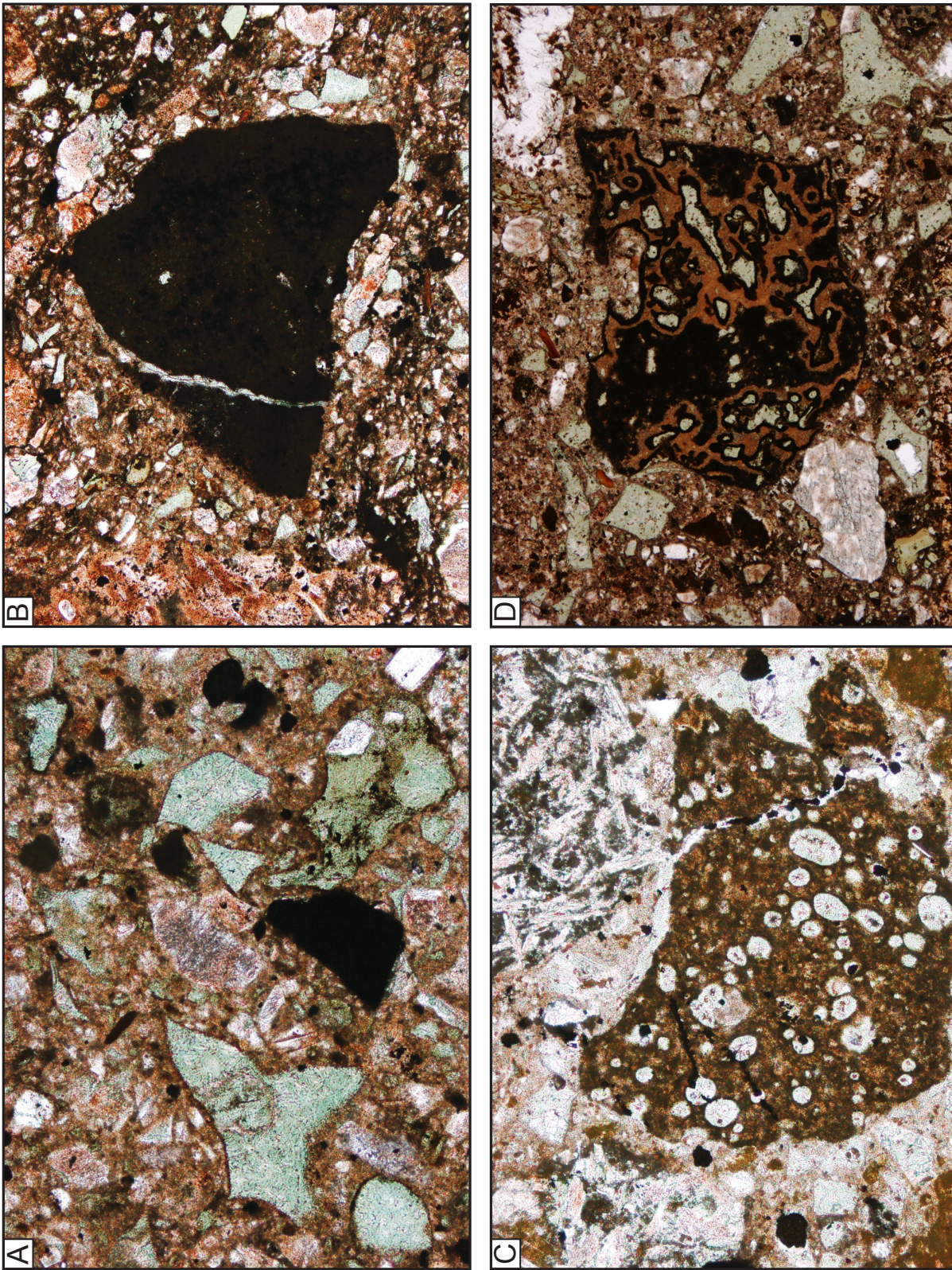


Figure 8. (A) Photomicrograph of breccia matrix showing sideromelane and tachylite pyroclasts. Sideromelane has been replaced by green clay and chlorite. Plane-polarized light; field of view ~1.3 mm across. (B) Photomicrograph of tachylite pyroclast with partly fluidal shape. Smaller sideromelane shards have been replaced by green clay. Plane-polarized light; field of view ~0.65 mm across. (C) Photomicrograph of moderately vesicular sideromelane pyroclast altered to brown palagonite. Pyroclast has partly fluidal outline. Plane-polarized light; field of view ~0.65 mm across. (D) Photomicrograph of sideromelane pyroclast altered to brown palagonite and showing partly aligned vesicles filled with green clay and chlorite. Sideromelane shards replaced by green clay are also visible. Plane-polarized light; field of view ~2.5 mm across.

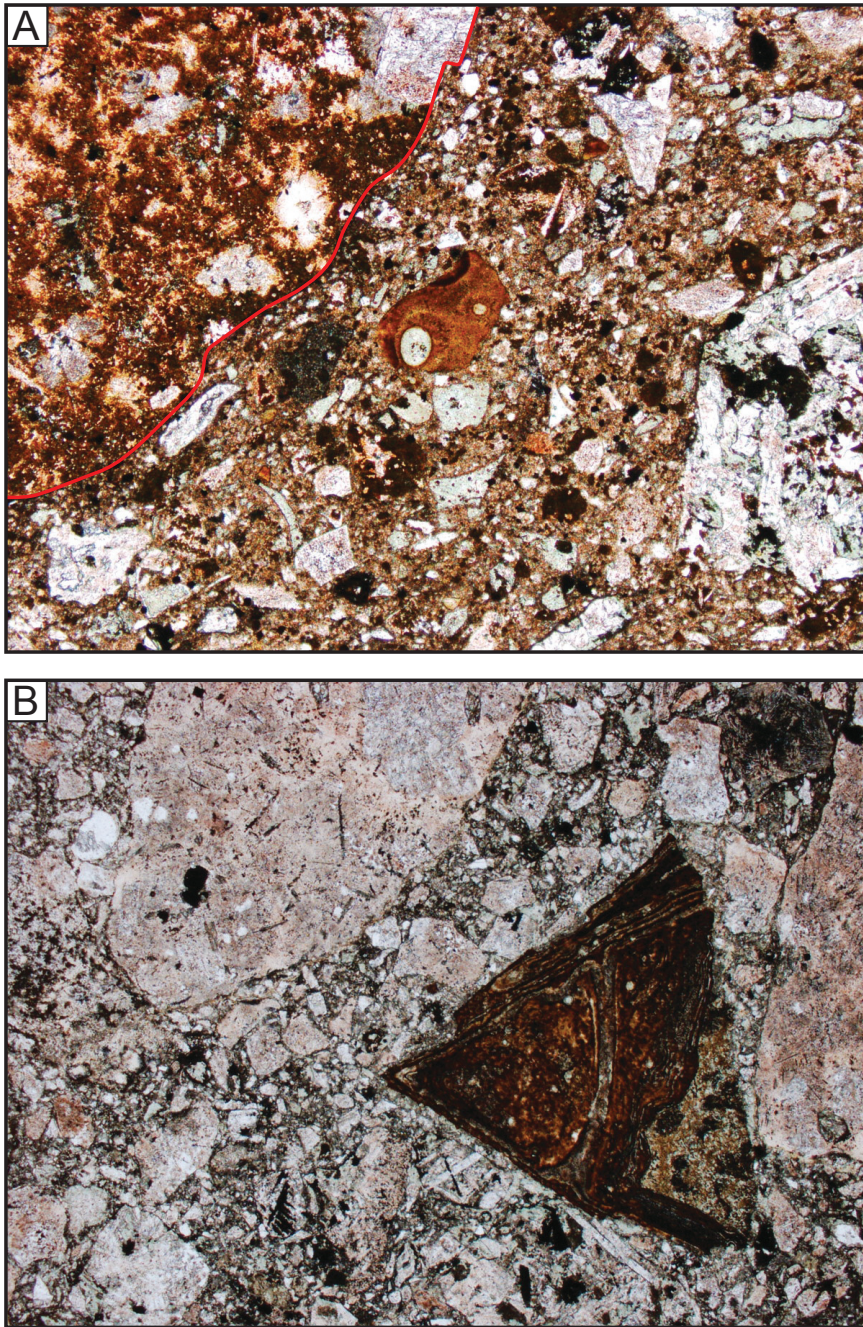


Figure 9. (A) Photomicrograph of sideromelane pyroclast altered to brown palagonite (center of view). Note vesicles present in pyroclast. A rhyolite clast is visible in upper left (margin is outlined). Plane-polarized light; field of view ~2 mm across. (B) Photomicrograph of poorly vesicular sideromelane pyroclast altered to brown palagonite. Pyroclast is intermixed with rhyolitic debris. Plane-polarized light; field of view ~2.5 mm across.

Timbered Hills (Fig. 13B). However, the two clasts plot together with many of the felsic rocks in the East Timbered Hills in the diagrams of Eby (1990, 1992) shown in Figure 14, indicating a similar involvement of older crust in their petrogenesis.

Price et al. (1998) analyzed six felsic lava samples within the Carlton Rhyolite in contact with the breccia and exposed in the quarry walls, and these samples are also plotted in Figures 10, 11A, 11B, and 12. Five of the samples are rhyolites and were collected at depths between 5 and 10 m below the unconformity with the Reagan Sandstone. Except in the case of TiO_2 , one of these samples consistently plots separately from the rest of the data in the Harker diagrams in Figure 10, having unusually high Al_2O_3 , FeO , and K_2O and unusually low MgO , CaO , Na_2O , and P_2O_5 . These differences indicate that this sample records more extreme alteration than the other samples. The remaining four samples tend to plot in an intermediate position between our rhyolite and microgranite clast samples and the East Timbered Hills felsic rocks in Figure 10. Addition of secondary carbonate probably explains the unusually high CaO content in two of the samples analyzed by Price et al. (1998) and shown in Figure 10. The sixth sample collected by those workers came from >30 m beneath the unconformity and has a broadly dacitic major-element composition, as seen in the Harker diagrams, with a lower silica content (63.49 wt %) than any of the other samples. In Figure 11A, this sample falls on the boundary between dacite/rhyodacite and trachyandesite fields. Immobile trace-element contents for the sample, however, are generally similar to those shown by the other felsic samples from the quarry (Figs. 11B and 12) and in some cases are nearly identical to the microgranite and rhyolite clasts in the breccia. In fact, all the analyzed felsic rocks from the quarry tend to fall near or overlap with Group 1 samples from the East Timbered Hills in the bivariate trace-element plots in Figure 12, implying that all these units have similar petrogenetic histories.

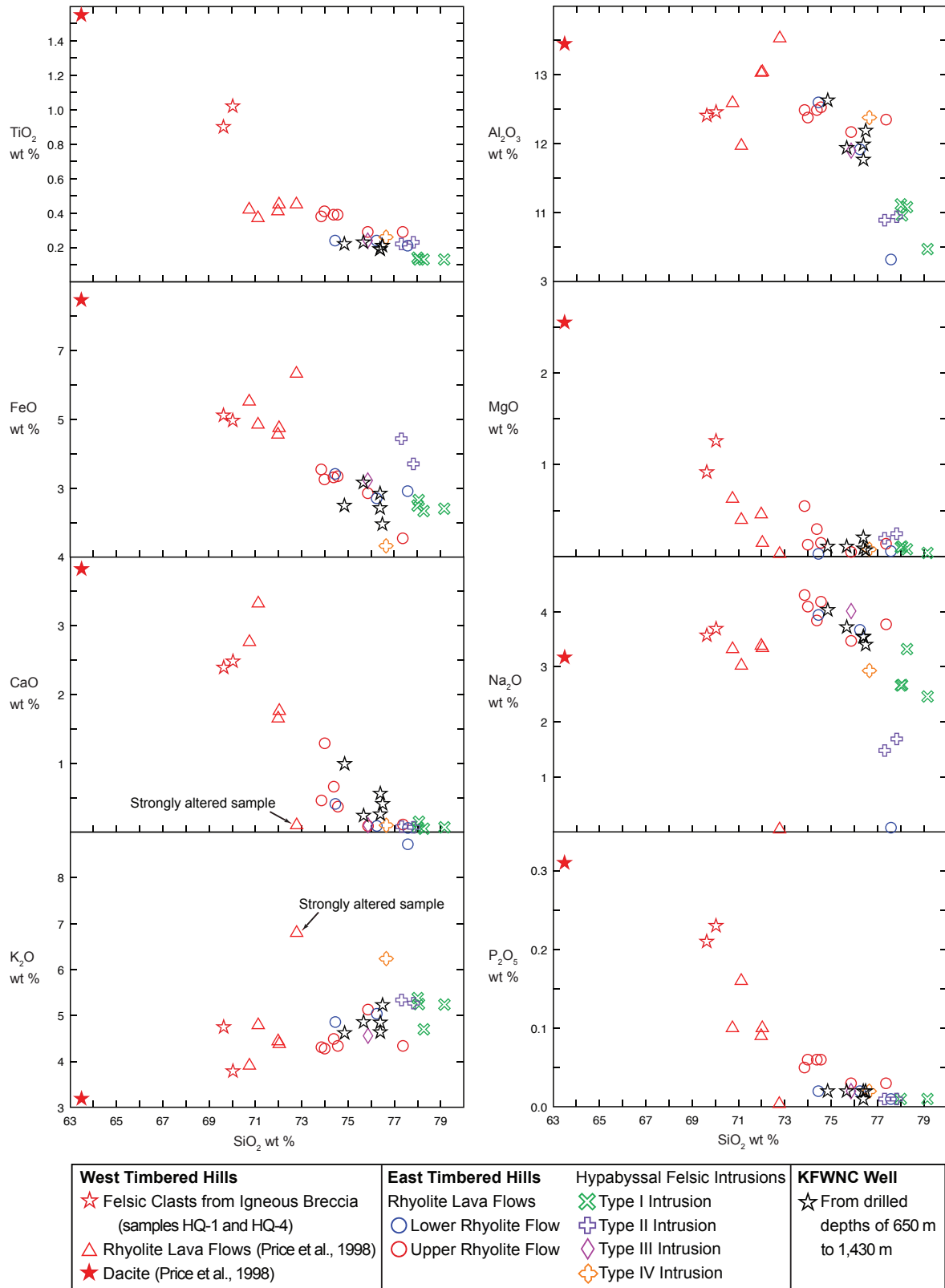


Figure 10. Harker variation diagrams for major elements in felsic samples from quarry; data from East Timbered Hills (Eschberger et al., this guidebook) are also shown for comparison. Strongly altered rhyolite sample analyzed by Price et al. (1998) is arrowed in CaO and K₂O diagrams.

Diabase

Our two analyses for the large diabase intrusion exposed in the quarry wall and for a representative diabase clast in the breccia are plotted in Harker diagrams in Figure 15 with data for three other diabase samples from the quarry analyzed by Price et al. (1998). For comparison purposes, we also show our data for diabase intrusions in the East Timbered Hills (Eschberger et al., this guidebook) and the general fields for diabase intrusions and the Roosevelt gabbros in the Wichita Mountains. It should be noted, however, that the Roosevelt gabbros in some cases exhibit cumulate textures as well as other evidence of internal fractional crystallization (Powell et al., 1980; Powell, 1986; Diez de Medina, 1988). Hence, samples of the gabbros probably do not in general represent liquid compositions.

Our sample of the large diabase intrusion in the quarry has the highest silica value (54.17 wt %) of any of the quarry diabases, in keeping with its relatively leucocratic nature, and has one of the highest silica values of the entire data set shown in Figure 15, being exceeded only by one Roosevelt Gabbro sample. At a given silica content, the diabase samples from the quarry have higher TiO₂, FeO, and P₂O₅ and lower MgO than the diabases from the East Timbered Hills. Based on the limited data available, it appears that these two suites of diabases evolved along different fractionation trends. The two suites also show some differences in CaO, Na₂O, and K₂O contents, but given the altered nature of the rocks, these differences could at least partly reflect secondary disturbance of the original igneous values. The latter possibility is consistent with the considerable scatter in the Harker diagrams for CaO, Na₂O, and K₂O in the samples analyzed by Price et al. (1998). Also, as noted by Eschberger et al. (this guidebook), petrographic evidence indicates that both CaO and K₂O have been affected by alteration in the diabases from the East Timbered Hills.

Complete trace-element and REE analyses are not available for the quarry diabase samples analyzed by Price et al. (1998), but the diabase intrusion and clast we analyzed show nearly identical patterns on the multi-element and REE plots in Figures 16A and 16B, indicating that the two samples represent magmas derived from the same source or reservoir. The only significant differences in these two patterns are the more pronounced negative Eu and Sr anomalies in the diabase intrusion sample, consistent with other evidence that this sample represents a more evolved composition than the diabase clast. The diabase intrusion and clast also plot very close together on the trace-element discrimination diagrams using immobile elements in Figures 16C, 16D, and 17, as does one of the diabase samples analyzed by Price et

al. (1998). These three samples consistently fall in fields for within-plate tholeiitic basalts in the discrimination diagrams. In contrast, the other two diabase samples analyzed by Price et al. (1998) and the East Timbered Hills diabases fall in fields for transitional or alkaline basalts.

DISCUSSION

We interpret the breccia exposed in the quarry to consist of pyroclastic debris formed by explosive volcanic processes. As suggested by Price et al. (1998), a major driving force for the explosions was violent subsurface interaction between mafic magma and groundwater. We infer that the variably vesicular sideromelane and tachylite fragments present in the breccia matrix are juvenile pyroclasts. The shapes of these pyroclasts are only partly controlled by broken bubble walls and record explosive phreatomagmatic behavior resulting from release of dissolved magmatic gases combined with rapid heating of external water to steam (e.g., Wohletz, 1983; Heiken and Wohletz, 1985; Ross and White, 2012). In some pyroclasts, elongate vesicles are truncated by planar clast margins (Fig. 8D) and record disruption of magma that was actively vesiculating as it was ascending in the conduit before being ripped apart by steam explosions.

Sideromelane glass is common in basaltic phreatomagmatic deposits and indicates rapid quenching of magma in contact with external water so that even tiny crystallites do not have time to form (Fisher and Schmincke, 1984). Tachylite is produced when less-rapid chilling of the magma allows time for crystallites of Fe-Ti oxide or pyroxene to develop, causing the turgid appearance of this kind of glass (Cas and Wright, 1987; McPhie et al., 1993). Many basaltic phreatomagmatic deposits described in the literature show mixtures of sideromelane and tachylite pyroclasts that record heterogeneous cooling rates in magma undergoing phreatomagmatic eruptions and/or recycling of pyroclasts with different cooling histories back into the conduit during repeated explosive activity (e.g., Houghton and Smith, 1993; Hanson and Elliot, 1996). A similar interpretation can be applied to the breccia in the Hanson Quarry.

The coarse size of many of the fragments in the breccia and the general lack of well-defined bedding are consistent with the interpretation that the breccia represents material filling the vent and/or underlying diatreme feeder conduit of a phreatomagmatic volcano (Fig. 18). The abundance of rhyolite and microgranite clasts suggests that explosive subsurface eruptions brecciated large amounts of country

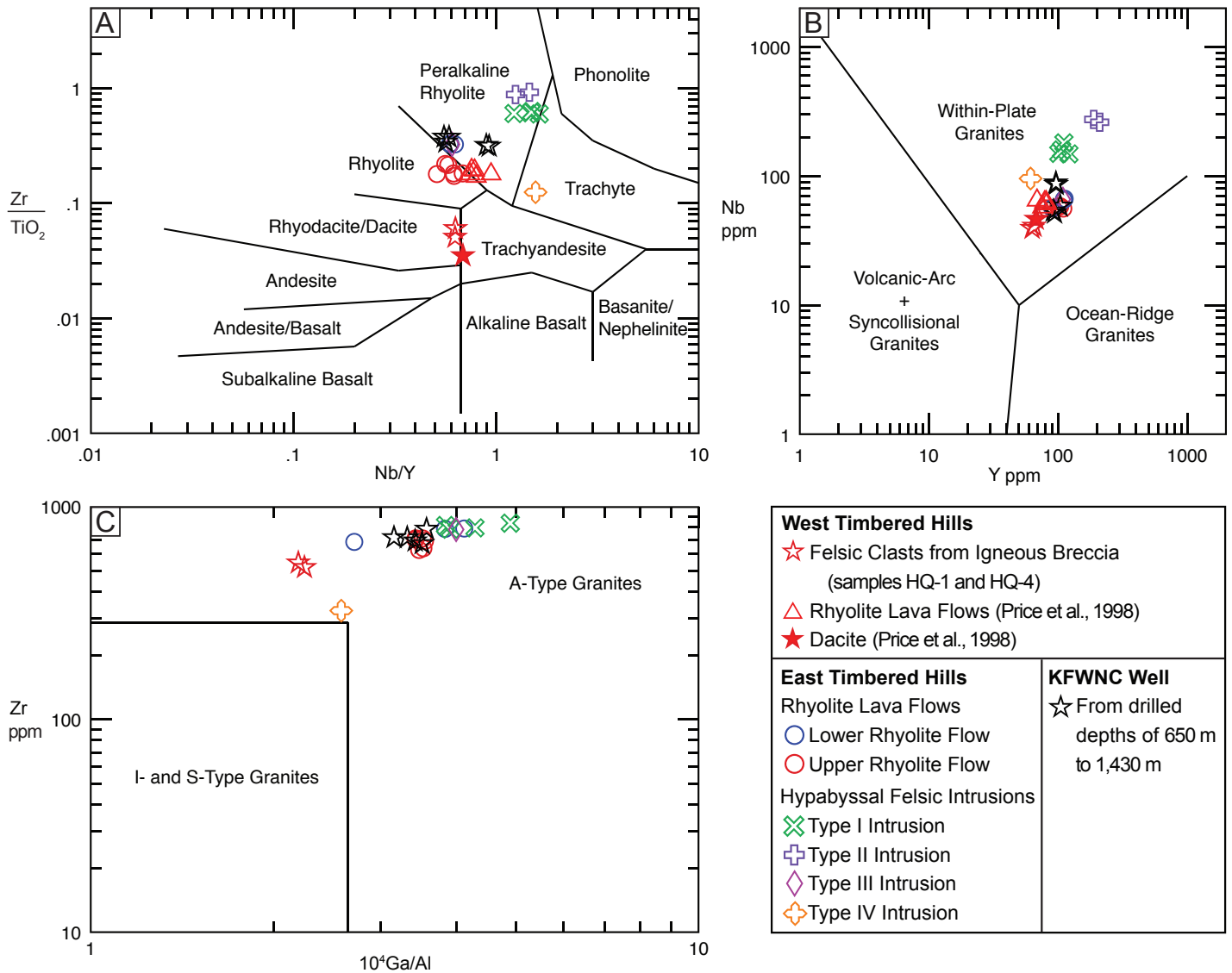


Figure 11. Felsic samples from quarry plotted on standard discrimination diagrams; data from East Timbered Hills (Eschberger et al., this guidebook) are also shown for comparison. (A) Zr/TiO₂ versus Nb/Y diagram of Winchester and Floyd (1977). (B) Nb versus Y diagram of Pearce et al. (1984). (C) Zr versus 10⁴Ga/Al diagram of Whalen et al. (1987).

rock, producing a type of phreatomagmatic volcano known as a maar, in which the crater cuts downward into bedrock, in some cases for considerable distances (Lorenz, 1986; White and Ross, 2011). Crude layering visible in the breccia in some of the quarry walls may represent proximal deposits of the ejecta rim to the crater which slumped downward into the growing vent (Fig. 18), as is commonly observed in maar-diatreme systems (White and Ross, 2011). Better constraints on the overall geometry and field relations of the breccia are needed before these interpretations can be rigorously tested.

We envision that events leading up to explosive generation of the breccia began when mafic magma intruded a sequence of extrusive rhyolite and related hypabyssal felsic rocks. Some initial batches of mafic magma must have formed intrusions large enough to undergo internal differentiation as shown by felsic segregations and igneous layering in some diabase clasts within the breccia. At some stage, the magma encountered groundwater-rich zones in the subsurface, leading to violent explosions. Fragmentation of the rhyolite and microgranite country rocks and early-formed diabase intrusions to form the abundant coarse

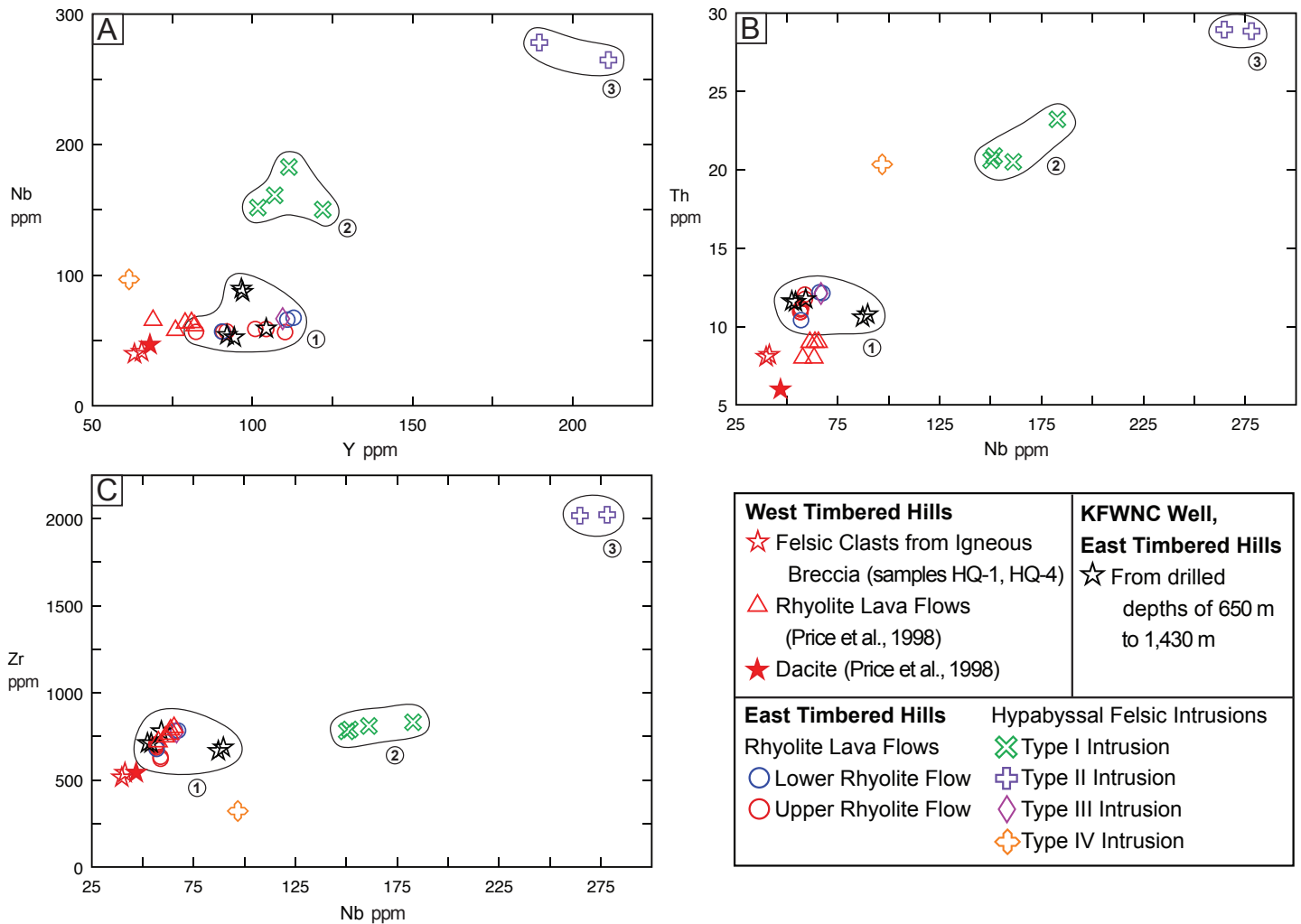


Figure 12. Bivariate trace-element plots for felsic samples from quarry; data from East Timbered Hills (Eschberger et al., this guidebook) are also shown for comparison, along with three distinct geochemical groups defined by that data. (A) Plot of Nb versus Y. (B) Plot of Th versus Nb. (C) Plot of Zr versus Nb.

lithic clasts in the breccia may have initially occurred solely by explosive steam generation from heated groundwater (e.g., Wohletz and Sheridan, 1983; White and Ross, 2011). However, the characteristics of the juvenile basaltic ash and lapilli in the breccia matrix indicate that the eruptive activity progressed to a stage where vesiculating basalt magma was being ripped apart by a combination of explosive release of dissolved magmatic volatiles and steam explosions from groundwater mixing with the fragmenting magma. Subrounded clasts within the breccia may have formed by abrasion within the diatreme during repeated explosive events. As noted previously, our analyses of a diabase clast within the breccia and of a large diabase intrusion that post-dates breccia formation reveal markedly similar contents of trace elements resistant to secondary alteration. Another

diabase intrusion sample analyzed by Price et al. (1998) is also geochemically similar to our samples. The fact that diabases with closely similar compositions were present both prior to the explosive activity that created the breccia and during subsequent non-explosive intrusion of diabase is consistent with the interpretation that mafic magma was the driving force for the explosions.

If our interpretation is correct, the igneous breccia and associated diabase intrusions exposed in the area of the quarry represent the only example of the vent and feeder system for a basaltic phreatomagmatic volcano so far documented within the Southern Oklahoma Aulacogen. As suggested by Price et al. (1998), explosive basaltic eruptive activity in this part of the aulacogen may have been favored by proximity to the rift-bounding Washita Valley

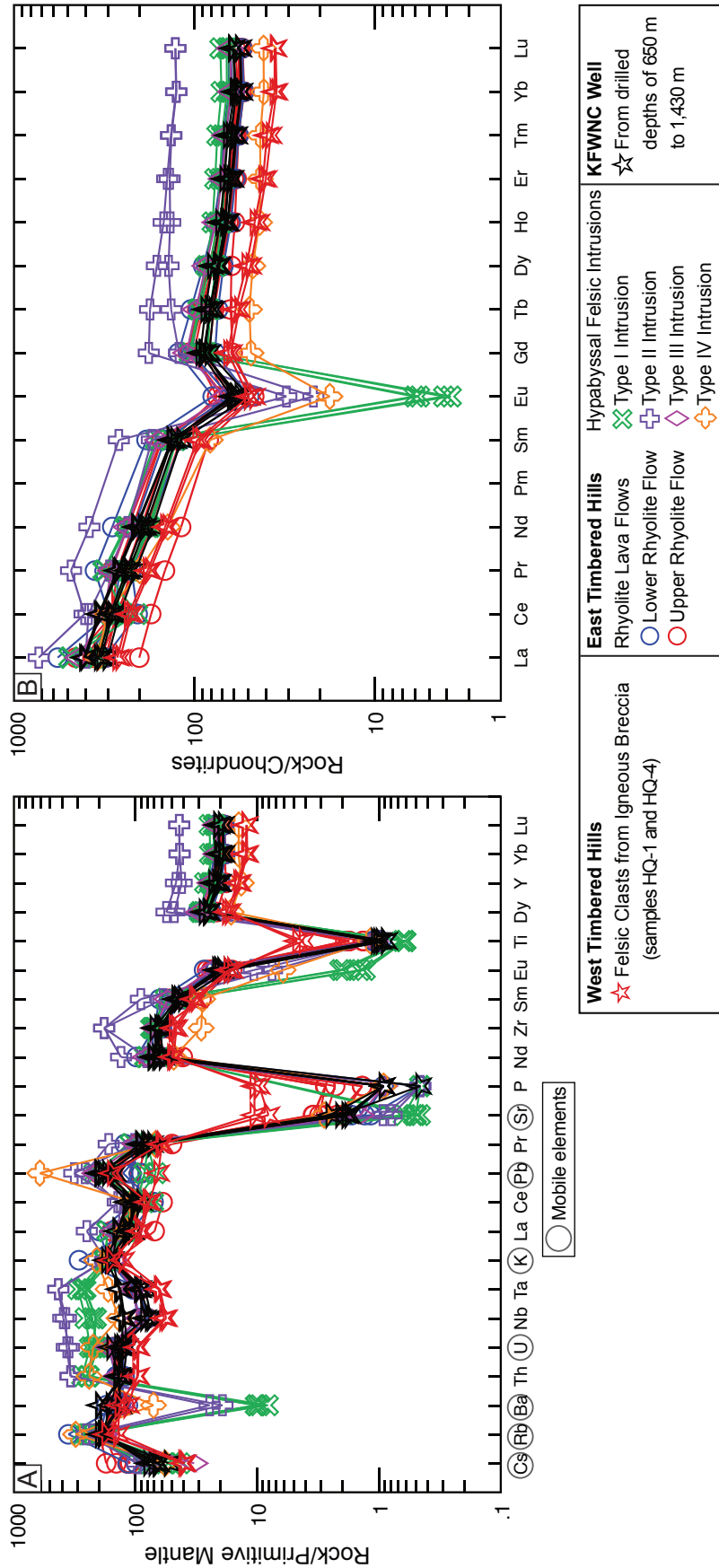


Figure 13. (A) Multi-element diagram for felsic samples from quarry. (B) REE diagram for felsic samples from quarry. Data from East Timbered Hills (Eschberger et al., this guidebook) are shown for comparison in both diagrams; normalization values are from Sun and McDonough (1989).

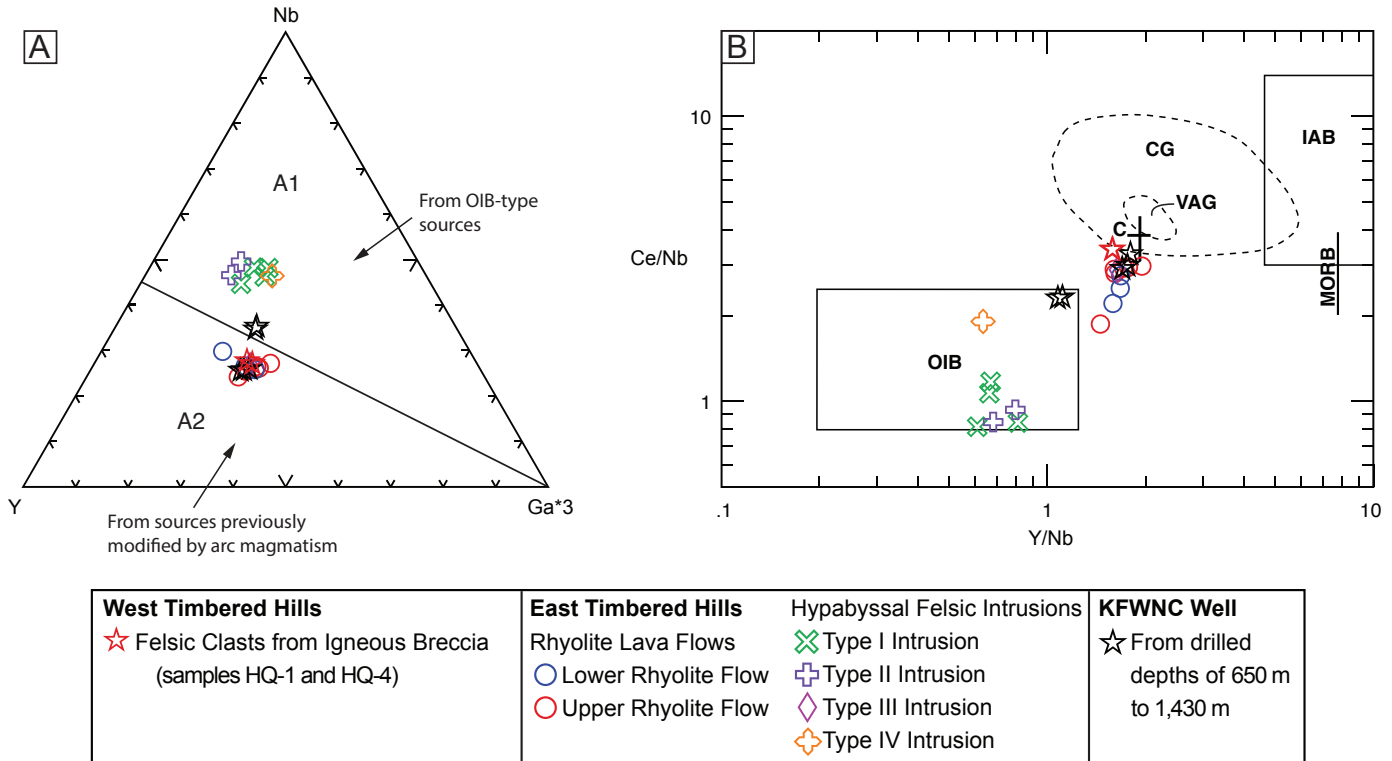


Figure 14. Felsic samples from quarry plotted on discrimination diagrams from Eby (1990, 1992) for A-type felsic rocks. (A) Y-Nb-Ga diagram. (B) Ce/Nb versus Y/Nb diagram; MORB: range for mid-ocean ridge basalts; IAB: field for island-arc basalts; cross labeled C: average crustal ratios; CG: field for syncollisional granites; VAG: field for volcanic-arc granites; OIB: field for ocean-island basalts.

Fault Zone, which allowed rising basalt magma to gain ready access to large volumes of groundwater. Recent work by Puckett et al. (this guidebook) shows that basaltic phreatomagmatic pyroclastic deposits are interbedded with rhyolite and basalt lavas near the subsurface extension of the Washita Valley Fault northwest of the Arbuckle outcrops. Ham et al. (1964) described similar deposits in one well that penetrated the Navajoe Mountain Basalt-Spilite Group farther northwest in the aulacogen. The results of these different studies suggest that explosive basaltic phreatomagmatic eruptions may have played an important role in the volcanic evolution of some parts of the aulacogen.

REFERENCES CITED

Aquilar, J., 1988, Geochemistry of mafic rock units of the Southern Oklahoma Aulacogen, southwestern Oklahoma [M.S. thesis]: Norman, Oklahoma, University of Oklahoma, 167 p.
 Befus, K.S., Hanson, R.E., Miggins, D.P., Breyer, J.A., and Busbey, A.B., 2009, Nonexplosive and explosive magma/wet-sediment interaction during emplacement of Eocene intrusions into Cretaceous to Eocene strata, Trans-Pecos igneous province, West Texas: Journal of Volcanology and Geothermal Research, v. 181, p. 155-172.

Bryan, W.B., 1972, Morphology of quench crystals in submarine basalts: Journal of Geophysical Research, v. 77, p. 5812-5819.
 Cas, R.A.F., and Wright, J.V., 1987, Volcanic Successions: Modern and Ancient: London, Allen, and Unwin, 528 p.
 DeGroat, P.J., Donovan, R.N., Hanson, R.E., and Weaver, B.L., 1995, Cambrian diabase and gabbro in the Blue Creek Canyon area, Wichita Mountains, southwestern Oklahoma: Oklahoma Geology Notes, v. 55, p. 168-186.
 Diez de Medina, D.M., 1988, Geochemistry of the Sandy Creek Gabbro, Wichita Mountains, Oklahoma [M.S. thesis]: Norman, Oklahoma, University of Oklahoma, 163 p.
 Eby, G.N., 1990, The A-type granitoids: A review of their occurrence and chemical characteristics and speculations on their petrogenesis: Lithos, v. 26, p. 115-134.
 Eby, G.N., 1992, Chemical subdivision of the A-type granitoids: Petrogenetic and tectonic implications: Geology, v. 20, p. 641-644.
 Elmore, R.D., Campbell, T., Banerjee, S., and Bixler, W.G., 1998, Palaeomagnetic dating of ancient fluid-flow events in the Arbuckle Mountains, southern Oklahoma, in Parnell, J., ed., Dating and Duration of Fluid Flow and Fluid-Rock Interaction: Geological Society of London Special Publication No. 144, p. 9-25.
 Eschberger, A.M., 2012, Volcanological and geochemical studies of Cambrian rift-related igneous rocks in the western Arbuckle Mountains, southern Oklahoma [M.S. thesis]: Fort Worth, Texas, Texas Christian University, 191 p.
 Fisher, R.V., and Schmincke H.-U., 1984, Pyroclastic Rocks: Berlin,

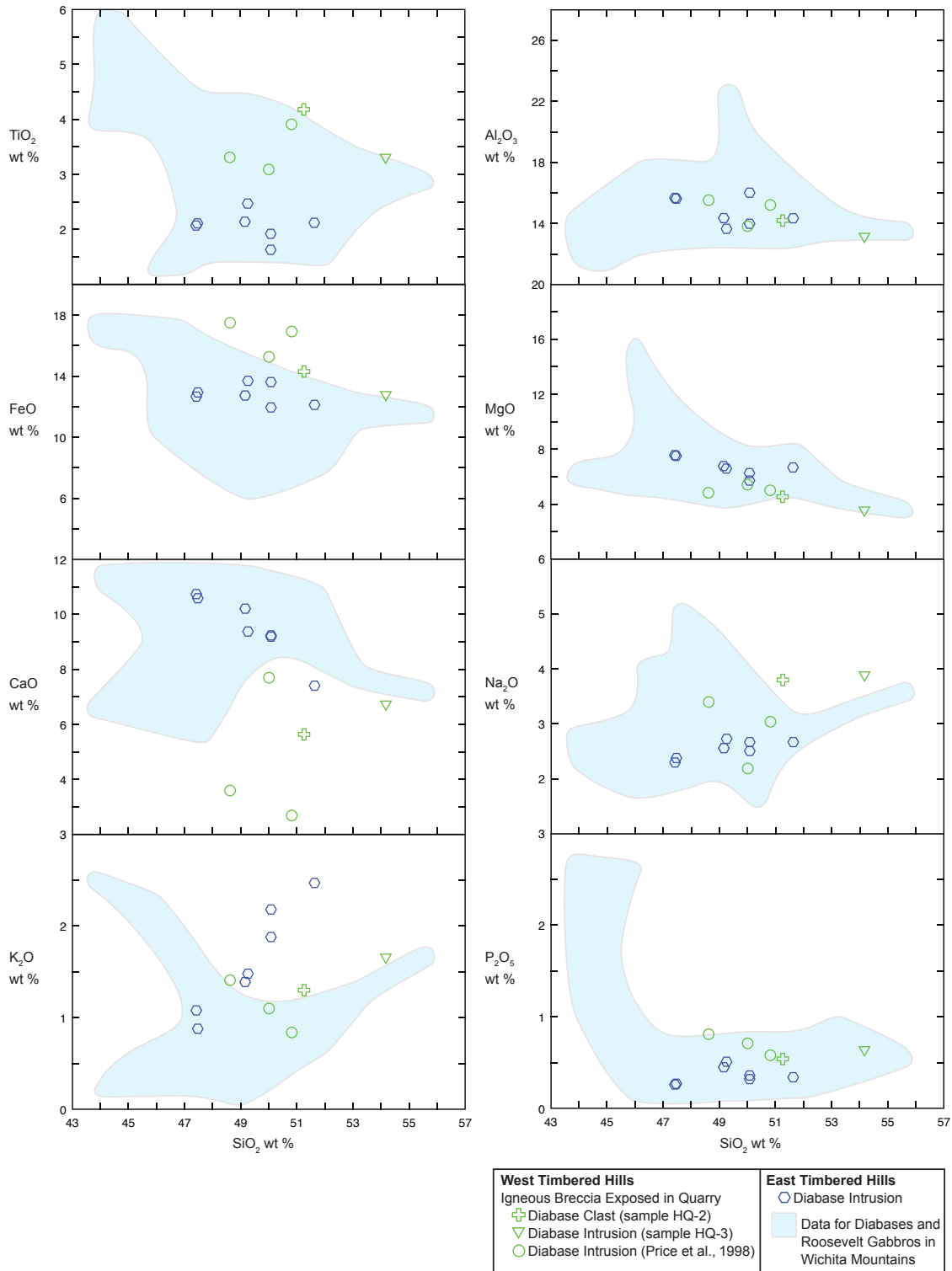


Figure 15. Harker variation diagrams for major elements in diabase samples from quarry; data from East Timbered Hills (Eschberger et al., this guidebook) are also shown for comparison. Blue fields represent data for diabase intrusions and Roosevelt gabbros in the Wichita Mountains from Aquilar (1988), DeGroat et al. (1995), and Diez de Medina (1988).

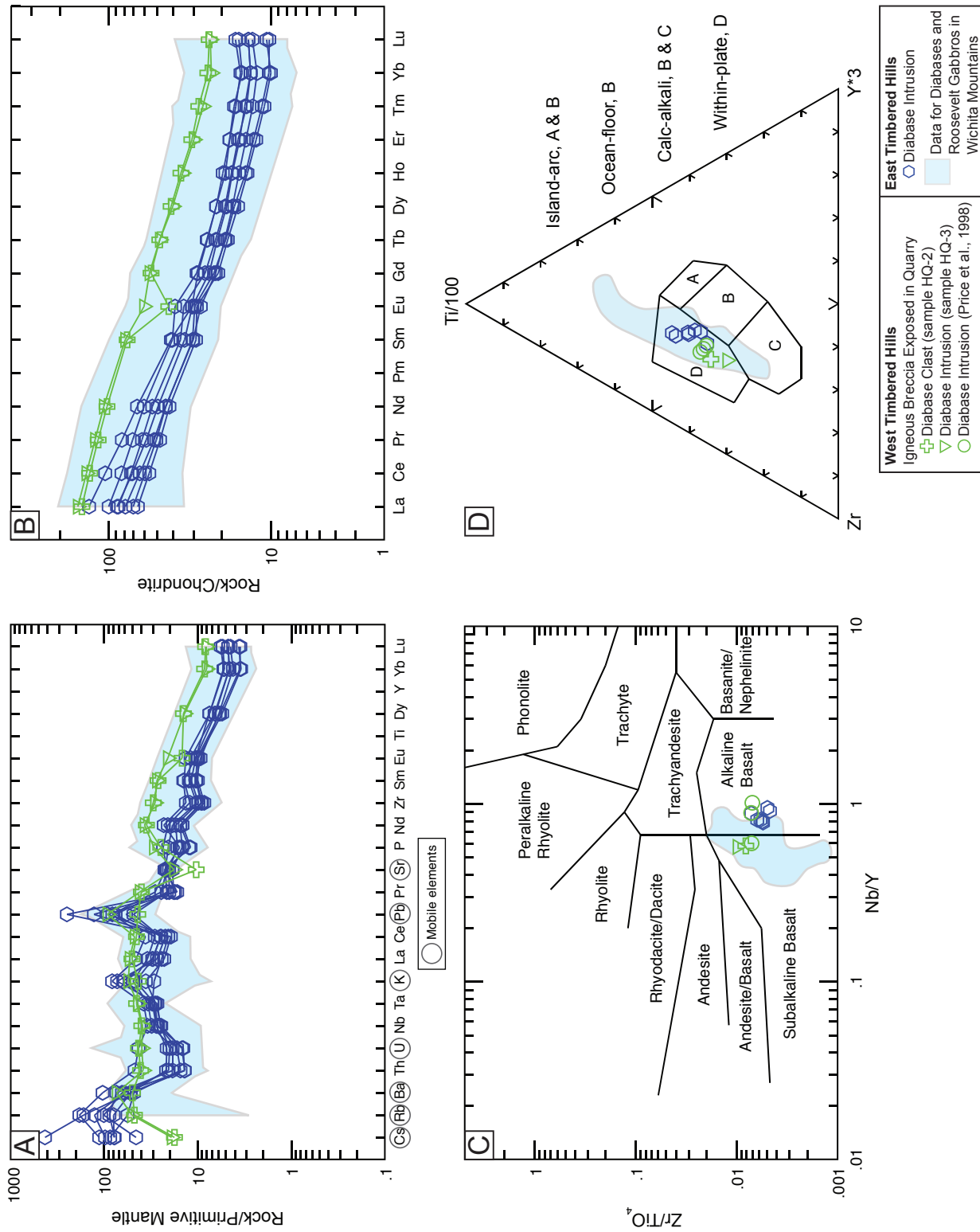


Figure 16. (A) Multi-element diagram for diabase samples from quarry. (B) REE diagram for diabase samples from quarry; normalization values in A and B from Sun and McDonough (1989). (C) Zr/TiO₂ versus Nb/Y diagram of Winchester and Floyd (1977). (D) Zr-Ti-Y diagram of Pearce and Cann (1973). Data from East Timbered Hills (Eschberger et al., this guidebook) are also shown for comparison. Blue fields represent data for diabase intrusions and Roosevelt gabbros in the Wichita Mountains from Aquilar (1988).

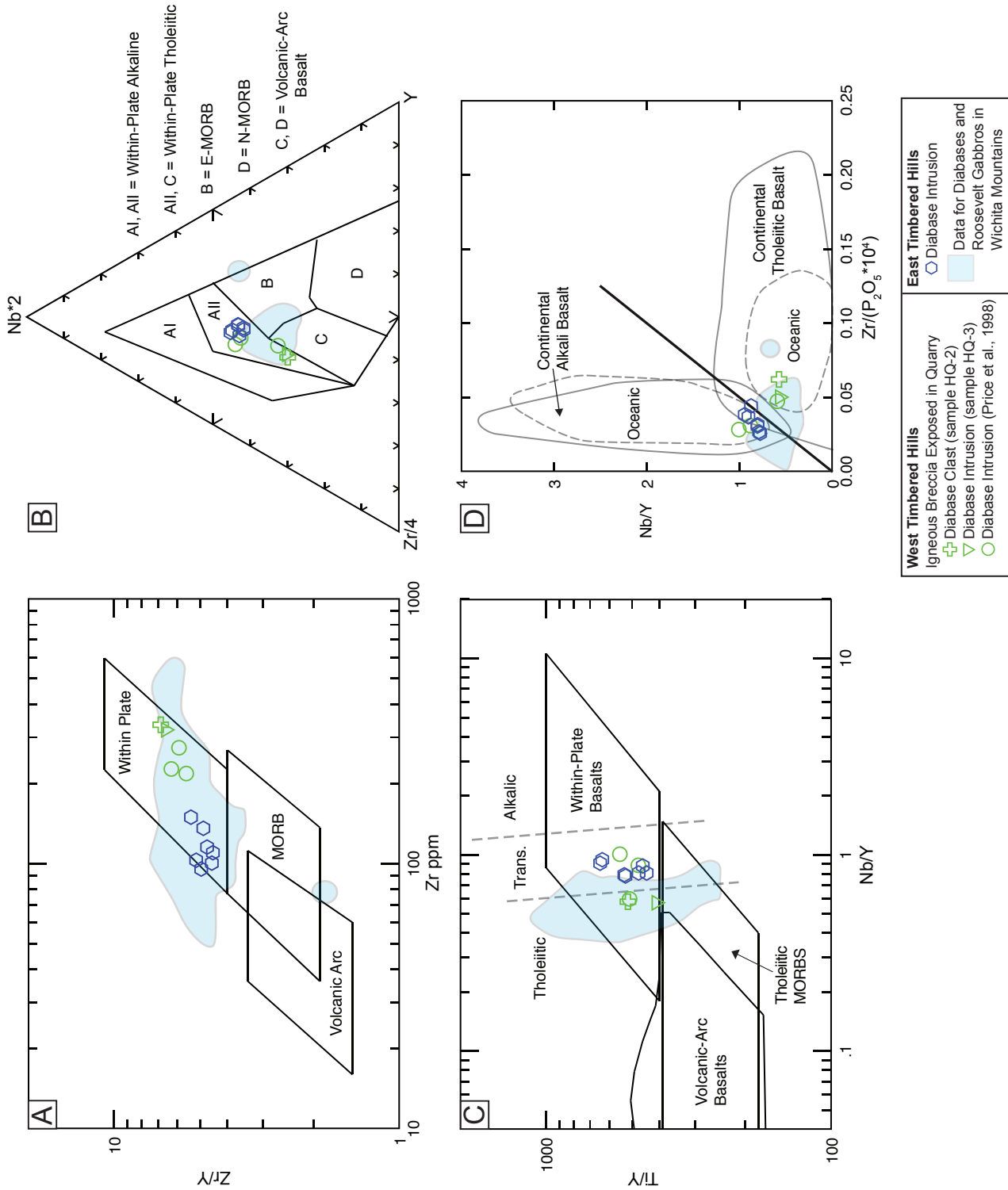


Figure 17. Diabase samples from quarry plotted on other standard discrimination diagrams. (A) Zr/Y versus Nb/Y diagram of Pearce and Norry (1979). (B) Zr/4-Nb*2-Y diagram of Meschede (1986). (C) Ti/Y versus Nb/Y diagram of Pearce (1982). (D) Nb/Y versus Zr/(P₂O₅*10⁴) diagram of Floyd and Winchester (1975). Blue fields represent data for diabase intrusions and Roosevelt gabbros in the Wichita Mountains from Aquilar (1988), DeGroat et al. (1995), and Diez de Medina (1988).

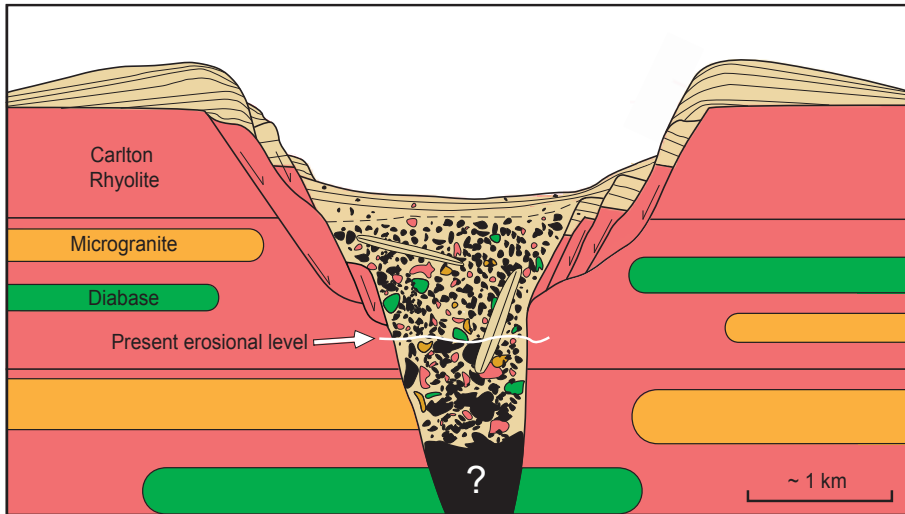


Figure 18. Model for formation of igneous breccia as the fill of a diatreme feeder to a maar volcano cutting into Carlton Rhyolite and microgranite and diabase intrusions. Modified from Befus et al. (2009).

- Springer-Verlag, 472 p.
- Floyd, P.A., and Winchester, J.A., 1975, Magma type and tectonic setting discrimination using immobile elements: *Earth and Planetary Science Letters*, v. 27, p. 211-218.
- Ham, W.E., Denison, R.E., and Merritt, C.A., 1964, Basement Rocks and Structural Evolution of Southern Oklahoma: *Oklahoma Geological Survey Bulletin* 95, 302 p.
- Hanson, R.E., and Elliot, D.H., 1996, Rift-related Jurassic basaltic phreatomagmatic volcanism in the central Transantarctic Mountains: Precursory stage to flood-basalt effusion: *Bulletin of Volcanology*, v. 58, p. 327-347.
- Heiken, G., and Wohletz, K., 1985, *Volcanic Ash*: Berkeley, University of California Press, 246 p.
- Houghton, B.F., and Smith, R.T., 1993, Recycling of magmatic clasts during explosive eruptions: Estimating the true juvenile content of phreatomagmatic volcanic deposits: *Bulletin of Volcanology*, v. 55, p. 414-420.
- Lorenz, V., 1986, On the growth of maars and diatremes and its relevance to the formation of tuff rings: *Bulletin of Volcanology*, v. 48, p. 265-274.
- McPhie, J., Doyle, M., and Allen, R., 1993, *Volcanic Textures: A Guide to the Interpretation of Textures in Volcanic Rocks*: University of Tasmania, Center for Ore Deposit and Exploration Studies, 196 p.
- Meschede, M., 1986, A method of discriminating between different types of mid-ocean ridge basalts and continental tholeiites with the Nb-Zr-Y diagram: *Chemical Geology*, v. 56, p. 207-218.
- Pearce, J.A., 1982, Trace element characteristics of lavas from destructive plate boundaries, in Thorpe, R.S., ed., *Andesites: Orogenic Andesites and Related Rocks*: New York, Wiley, p. 525-548.
- Pearce, J.A., and Cann, J.R., 1973, Tectonic setting of basic volcanic rocks determined using trace element analyses: *Earth and Planetary Science Letters*, v. 19, p. 290-300.
- Pearce, J.A., and Norry, M.J., 1979, Petrogenetic implications of Ti, Zr, Y and Nb variations in volcanic rocks: *Contributions to Mineralogy and Petrology*, v. 69, p. 33-47.
- Pearce, J.A., Harris, N.B.W., and Tindle, A.G., 1984, Trace element discrimination diagrams for the tectonic interpretation of granitic rocks: *Journal of Petrology*, v. 25, p. 956-983.
- Powell, B.N., 1986, The Raggedy Mountain Gabbro Group, in Gilbert, M.C., ed., *Petrology of the Cambrian Wichita Mountains Igneous Suite*: Oklahoma Geological Survey Guidebook 23, p. 21-52.
- Powell, B.N., Gilbert, M.C., and Fischer, J.F., 1980, Lithostratigraphic Classification of basement rocks of the Wichita province, Oklahoma: *Geological Society of America Bulletin*, v. 91, Part I, Summary, p. 509-514; Part II, p. 1875-1994.
- Price, J.D., Hogan, J.P., Gilbert, M.C., and Denison, R.E., 1998, Field guide to the basement rocks of the Southern Oklahoma aulacogen: Guidebook, South-Central Meeting of the Geological Society of America, March 20-24, Norman, University of Oklahoma, 89 p.
- Ross, P.-S., and White, J.D.L., 2012, Quantification of vesicle characteristics in some diatreme-filling deposits, and the explosivity levels of magma-water interactions within diatremes: *Journal of Volcanology and Geothermal Research*, v. 245-246, p. 55-67.
- Shelley, D., 1993, *Igneous and Metamorphic Rocks under the Microscope*: London, Chapman & Hall, 445 p.
- Sun, S.S., and McDonough, W.F., 1989, Chemical and isotopic systematics of oceanic basalts; implications for mantle composition and process, in Saunders, A.D., and Norry, M.J., eds., *Magmatism in the Ocean Basins*: Geological Society of London Special Publication 42, p. 313-345.
- Uhl, B.F., 1932, *Igneous rocks of the Arbuckle Mountains* [M.S. thesis]: Norman, Oklahoma, University of Oklahoma, 54 p.
- Whalen, J.B., Currie, K.L., and Chappell, B.W., 1987, A-type granites: Geochemical characteristics, discrimination and petrogenesis: *Contributions to Mineralogy and Petrology*, v. 95, p. 407-419.
- White, J.D.L., and Ross, P.-S., 2011, Maar-diatreme volcanoes: A review: *Journal of Volcanology and Geothermal Research*, v. 201, p. 1-29.
- Winchester, J.A., and Floyd, P.A., 1977, Geochemical discrimination of different magma series and their differentiation products using immobile elements: *Chemical Geology*, v. 20, p. 325-343.
- Wohletz, K.H., 1983, Mechanisms of hydrovolcanic pyroclast formation: Grain size, scanning electron microscopy, and experimental studies: *Journal of Volcanology and Geothermal Research*, v. 17, p. 31-63.
- Wohletz, K.H., and Sheridan, M.F., 1983, Hydrovolcanic explosions II. Evolution of basaltic tuff rings and tuff cones: *American Journal of Science*, v. 283, p. 385-413.
- Zavala, K., Leitch, A.M., and Fisher, G.W., 2011, Silicic segregations of the Ferrar dolerite sills, Antarctica: *Journal of Petrology*, v. 52, p. 1927-1964.

